Received: 5 March 2023 | Revised: 18 April 2023 | Accepted: 25 April 2023

DOI: 10.1002/sus2.131

SusMat WILEY

REVIEW

Design of earth-abundant amorphous transition metal-based catalysts for electrooxidation of small molecules: Advances and perspectives

Zhijie Chen[1] | **Ning Han**[2] | **Renji Zheng**[3] | **Zijie Ren**[4] | **Wei Wei**[1] | **Bing-Jie Ni**[1]

[1]Centre for Technology in Water and Wastewater, School of Civil and Environmental Engineering, University of Technology Sydney, Ultimo, New South Wales, Australia

[2]Department of Materials Engineering, KU Leuven, Leuven, Belgium

[3]School of Minerals Processing and Bioengineering, Central South University, Changsha, Hunan, China

[4]School of Resources and Environmental Engineering, Wuhan University of Technology, Wuhan, China

Correspondence
Bing-Jie Ni, Centre for Technology in Water and Wastewater, School of Civil and Environmental Engineering, University of Technology Sydney, Ultimo 2007, NSW, Australia.
Email: bingjieni@gmail.com

Funding information
Australian Research Council, Grant/Award Number: DP220101139

Abstract

Electrochemical oxidation of small molecules (e.g., water, urea, methanol, hydrazine, and glycerol) has gained growing scientific interest in the fields of electrochemical energy conversion/storage and environmental remediation. Designing cost-effective catalysts for the electrooxidation of small molecules (ESM) is thus crucial for improving reaction efficiency. Recently, earth-abundant amorphous transition metal (TM)-based nanomaterials have aroused souring interest owing to their earth-abundance, flexible structures, and excellent electrochemical activities. Hundreds of amorphous TM-based nanomaterials have been designed and used as promising ESM catalysts. Herein, recent advances in the design of amorphous TM-based ESM catalysts are comprehensively reviewed. The features (e.g., large specific surface area, flexible electronic structure, and facile structure reconstruction) of amorphous TM-based ESM catalysts are first analyzed. Afterward, the design of various TM-based catalysts with advanced strategies (e.g., nanostructure design, component regulation, heteroatom doping, and heterostructure construction) is fully scrutinized, and the catalysts' structure-performance correlation is emphasized. Future perspectives in the development of cost-effective amorphous TM-based catalysts are then outlined. This review is expected to provide practical strategies for the design of next-generation amorphous electrocatalysts.

KEYWORDS

amorphous catalysts, catalyst design, electrocatalytic conversion, electrochemical oxidation, transition metals

1 | INTRODUCTION

The electrooxidation of small molecules (ESM) is a favorable way to oxidize small molecules into target substances with the merits of high reaction efficiency and selectivity, simple operation conditions, no need for external oxidants, and environmental friendliness.[1] Of note, ESM plays a central role in advanced energy systems

and environmental remediation techniques. For example, water oxidation, namely, the oxygen evolution reaction (OER), is a key reaction in water electrolysis-driven hydrogen production techniques and metal–air batteries.[2] The urea/hydrazine oxidation reaction (UOR/HzOR) is important for urine/hydrazine wastewater purification and direct urea/hydrazine fuel cells.[3] Moreover, coupling UOR/HzOR with hydrogen evolution reaction (HER) is suggested to realize energy-saving hydrogen production.[4] Similarly, the electrochemical oxidation of methanol, glycerol, sulfion, formic acid, and 5-hydroxymethylfurfural (HMF) also has been investigated to replace OER for producing hydrogen with lower energy consumption and obtaining value-added chemicals.[5,6] Overall, the oxidative transformation of these small molecules in an electrochemical way would significantly benefit the sustainable energy system and green environment.

ESM generally shows a multi-electron reaction characteristic and leads to high-energy barriers. Therefore, it is important to boost the ESM process with efficient electrocatalysts. Precious metals (e.g., Ru, Ir, Pd, Rh, and Pt)-based catalysts have shown high catalytic activities and good durability,[7,8] but their high prices and low reserves severely hamper their applications.[9,10] Alternatively, catalysts based on abundant transition metals (TMs, e.g., Fe, Ni, and Co) have shown promising catalytic performance for ESM,[11] especially in alkaline or neutral electrolytes. Great efforts have thus been made to exploit cost-efficient TM-based ESM catalysts.

Thousands of TM-based catalysts with diverse nanostructures, crystal structures, and compositions have been developed. Among them, catalysts with an amorphous phase have attracted enormous scientific attention due to their flexible crystal/electronic structures, rich electroactive sites, and so on. Thus, amorphous catalysts show better electrochemical performance for ESM than crystalline counterparts.[12] To upgrade the catalytic performance of amorphous catalysts, efficient strategies have been adopted to populate the catalytically active sites and/or improve the intrinsic catalytic activity of catalysts, such as nanostructure design, component regulation, heteroatom doping, and heterostructure construction. For example, the catalytic activity of copper hydroxide toward HMF oxidation can be significantly enhanced by forming a heterostructure with nickel hydroxide.[13] This is because the presence of nickel hydroxide can enrich the active sites for HMF oxidation. By utilizing these powerful strategies, many efficient catalysts based on amorphous TM alloys, (hydr)oxides, chalcogenides, phosphides, nitrides, borides, and oxometallates have been developed for ESM (Scheme 1 and Table 1). These amorphous materials significantly enrich the ESM catalyst community and largely promote related reaction processes. In consequence, the great interest in this topic hastens a comprehensive summary covering the design of amorphous TM-based ESM electrocatalysts.

This review aims to deliver a critical examination of recent advancements in the design of amorphous

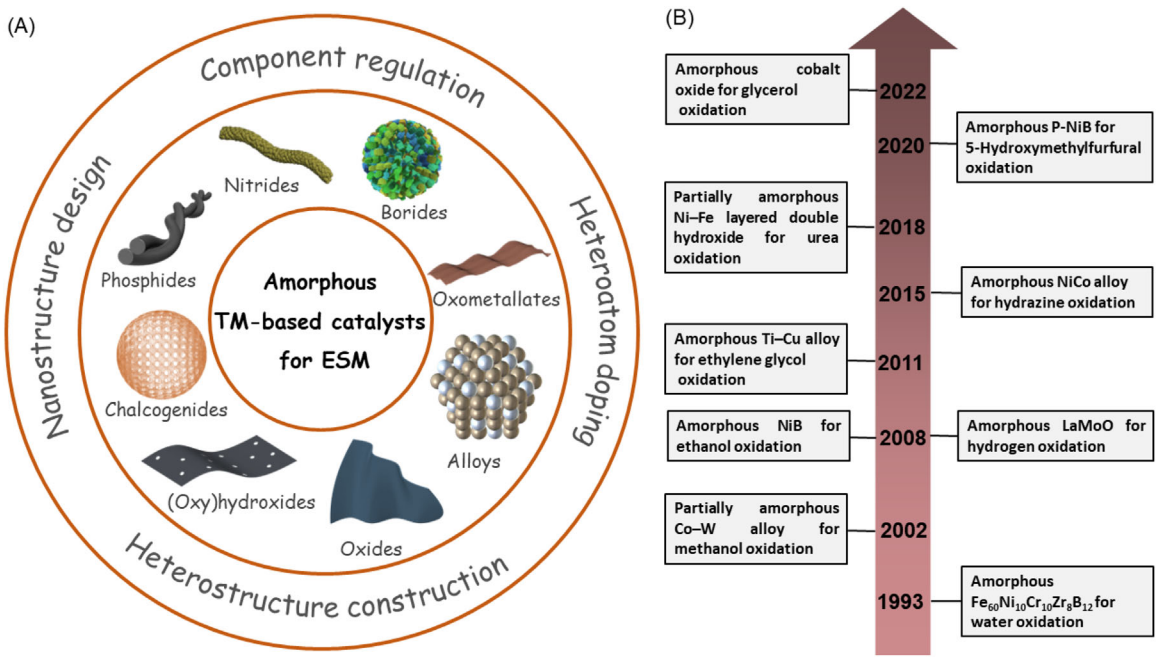

SCHEME 1 (A) Design of amorphous transition metal (TM)-based catalysts for electrooxidation of small molecules (ESM). (B) Milestone timeline of studies related to amorphous TM-based catalysts for ESM.[14–22]

TABLE 1 Representative amorphous transition metal (TM)-based electrocatalysts for electrooxidation of small molecules (ESM)

Electrocatalyst	Design strategy	Reaction	Electrolyte	Performance
Amorphous FeCoNi alloy aerogel[23]	Nanostructure design	OER	1 M KOH	η_{10} = 235 mV[a], Tafel slope = 50 mV dec^{-1}
Amorphous NiFe alloy/MoS_2[24]	Heterostructure construction	OER	1 M KOH	η_{10} = 260 mV, Tafel slope = 48 mV dec^{-1}
Amorphous $Co_8Ce_2O_x$[25]	Component regulation	EOHMF[b]	5 mM HMF + 1 M KOH	92% DFF[c] selectivity at 1.5 V vs. RHE[d]
Fe-doped amorphous CoO_x[26]	Heteroatom doping	OER	1 M KOH	η_{10} = 280 mV, Tafel slope = 39.9 mV dec^{-1}
Co/amorphous $LaCoO_x$@N-C[27]	Heterostructure construction	HzOR	0.1 M hydrazine + 1 M KOH	j[e] = 69.2 mA cm^{-2} at 0.3 V vs. RHE
NiO/amorphous CrO_x[28]	Heterostructure construction	UOR	0.33 M urea + 1 M KOH	j = 10 mA cm^{-2} at 1.32 V vs. RHE
$Ni(OH)_2$/amorphous $Cu(OH)_2$[13]	Heterostructure construction	EOHMF	5 mM HMF + 1 M KOH	91.2% FDCA[f] yield at 1.45 V vs. RHE
Amorphous FeOOH/V-doped NiS[29]	Heterostructure construction, heteroatom doping	OER	1 M KOH	η_{100} = 225 mV, Tafel slope = 75 mV dec^{-1}
Amorphous $CoS_x(OH)_y$/Ti[30]	Heterostructure construction, nanostructure design	UOR	0.5 M urea + 1 M KOH	j = 10 mA cm^{-2} at 1.3 V vs. RHE
Amorphous CoNi LDH[g] nanosheets[31]	Nanostructure design	OER	1 M KOH	η_{10} = 280 mV, Tafel slope = 28 mV dec^{-1}
Partially amorphous Ni–Fe LDH[20]	Component regulation	UOR	0.33 M urea + 1 M KOH	j = 30 mA cm^{-2} at 1.362 V vs. RHE
Amorphous CoO_xH_y[32]	Nanostructure design	GOR[h]	0.1 M borate buffer solution + 0.05 M glycerol	HPA[i] production rate of 679.2 μmol min^{-1} $m_{geo}{}^{-2}$
Amorphous $Ni(OH)_2$/Ni phosphate[33]	Heterostructure construction	OER	pH 7.2	η_{10} = 340 mV, Tafel slope = 175 mV dec^{-1}
NiTe/amorphous NiS[34]	Heterostructure construction, nanostructure design	UOR	0.33 M urea + 1 M KOH	j = 10 mA cm^{-2} at 1.31 V vs. RHE
Amorphous MoS_2/CoS/$Co_{0.85}Se$ nanotube arrays[35]	Heterostructure construction, nanostructure design	UOR	0.5 M urea + 1 M KOH	j = 50 mA cm^{-2} at 1.38 V vs. RHE
Amorphous Ni–Fe–Se hollow nanospheres[36]	Nanostructure design	OER	1 M KOH	η_{100} = 222 mV, Tafel slope = 39 mV dec^{-1}
Cu-doped amorphous $NiSe_x$/crystalline $NiSe_2$[37]	Heterostructure construction, nanostructure design, heteroatom doping	OER	1 M KOH	η_{10} = 339 mV, Tafel slope = 54.2 mV dec^{-1}
Ni@amorphous NiP/C[38]	Heterostructure construction	HzOR	0.1 M hydrazine + 1 M KOH	2675.1 A $g_{Ni}{}^{-1}$@0.25 V vs. RHE
Ni(Cu) alloy@amorphous NiFeP[39]	Heterostructure construction	HzOR	0.5 M hydrazine + 1 M KOH	η_{10} = 6 mV, Tafel slope = 48.1 mV dec^{-1}
Amorphous $Ni_{40}Fe_{40}P_{20}$[40]	Component regulation	OER	0.05 M H_2SO_4	η_{10} = 540 mV
Amorphous Ni_2P/graphene[41]	Heterostructure construction	UOR	0.5 M urea + 1 M KOH	j = 10 mA cm^{-2} at 1.28 V vs. RHE
Amorphous W, P co-doped FeB[42]	Heteroatom doping	OER	1 M KOH	η_{10} = 209 mV, Tafel slope = 39 mV dec^{-1}
Amorphous porous Ni–B/C[43]	Nanostructure design	HzOR	0.02 M hydrazine + 1 M KOH	1495 A $g_{Ni}{}^{-1}$@0.2 V vs. RHE
Amorphous Fe-doped $InPO_4$ nanosheets[44]	Nanostructure design, heteroatom doping	OER	1 M KOH	η_{10} = 230 mV, Tafel slope = 46 mV dec^{-1}
Amorphous Fe/Ni biphosphate[45]	Nanostructure design	MOR[j]	80 mM methanol + 1 M KOH	j = 40.25 mA cm^{-2} at 0.472 V
N-doped amorphous CoFe selenites[46]	Heteroatom doping	OER	1 M KOH	η_{10} = 242 mV, Tafel slope = 59.1 mV dec^{-1}

(Continues)

TABLE 1 (Continued)

Electrocatalyst	Design strategy	Reaction	Electrolyte	Performance
Amorphous NiCo-borate nanosheet arrays[47]	Nanostructure design	OER	0.1 M K-Bi[k]	η_{10} = 430 mV, Tafel slope = 92 mV dec^{-1}
Amorphous CoFePO$_x$/crystalline Ni(PO$_3$)$_2$[48]	Heterostructure construction	OER	1 M KOH	η_{10} = 213 mV, Tafel slope = 39 mV dec^{-1}
Amorphous CoFe phyllosilicates[49]	Component regulation	OER	1 M KOH	η_{10} = 329 mV, Tafel slope = 34.3 mV dec^{-1}

Abbreviations: HMF, 5-hydroxymethylfurfural; HzOR, hydrazine oxidation reaction; OER, oxygen evolution reaction; RHE, reversible hydrogen electrode; UOR, urea oxidation reaction.

[a]Overpotential at the current density of 10 mA cm^{-2}.
[b]Electrochemical oxidation of HMF.
[c]2,5-Diformylfuran.
[d]Reversible hydrogen electrode.
[e]Current density.
[f]2,5-Furandicarboxylic acid.
[g]Layered double hydroxide.
[h]Glycerol oxidation reaction.
[i]Hydroxypyruvic acid.
[j]Methanol oxidation reaction.
[k]Potassium borate.

TM-based ESM catalysts. Instead of listing previous work, this review mainly focuses on the application of diverse catalyst design strategies in the development of efficient ESM electrocatalysts. First, the critical structural/electronic features of amorphous catalysts are analyzed. Then, the designs of amorphous TM alloys, (hydr)oxides, chalcogenides, phosphides, nitrides, borides, and oxometallates are detailed, with representative examples interpreted. Moreover, perspectives on the development of amorphous ESM catalysts are pointed out.

2 | FEATURES OF AMORPHOUS ELECTROCATALYSTS

Amorphous catalysts possess unique characteristics of short-range order and long-range disorder and thereby manifest different physicochemical properties from their crystalline analogs.[50,51] Generally, the better catalytic performance of amorphous catalysts than their crystalline counterparts can be explained by their following features, namely, large specific surface area (SSA), flexible electronic structure, and deep structure reconstruction during the ESM process.

3 | Large specific surface area

Compared with crystalline materials that generally synthesized at relatively high temperatures, amorphous materials prepared at mild conditions generally show higher SSA.[52,53] A main reason is that the amorphous-to-crystalline conversion process would lead to particle coarsening during the high-temperature process.[54] This feature of amorphous catalysts guarantees more electroactive sites and a larger electrochemical active surface area (ECSA) and promotes the interaction between catalysts and reactants/intermediates.[50,55] As reported by Cai et al., the amorphous NiFe alloy synthesized at room temperature comprises interconnected nanoparticles with an average size of 50 nm (Figure 1A,B), which is smaller than the crystalline counterpart prepared at 600°C (100 nm, Figure 1C,D).[56] The amorphous catalysts with smaller size exhibit higher SSA, which can promote mass/charge transfer and provides abundant transportation channels for electrolytes and gas products.[57] The high SSA of amorphous TM-based catalysts also results in larger ECSA (Figure 1E), and smaller Tafel slopes (Figure 1F), thereby faster reaction kinetics.[56] As a large SSA ensures better contact at the catalyst–electrolyte interface, amorphous catalysts show smaller charge transfer resistance (R_{ct}) than crystalline materials.

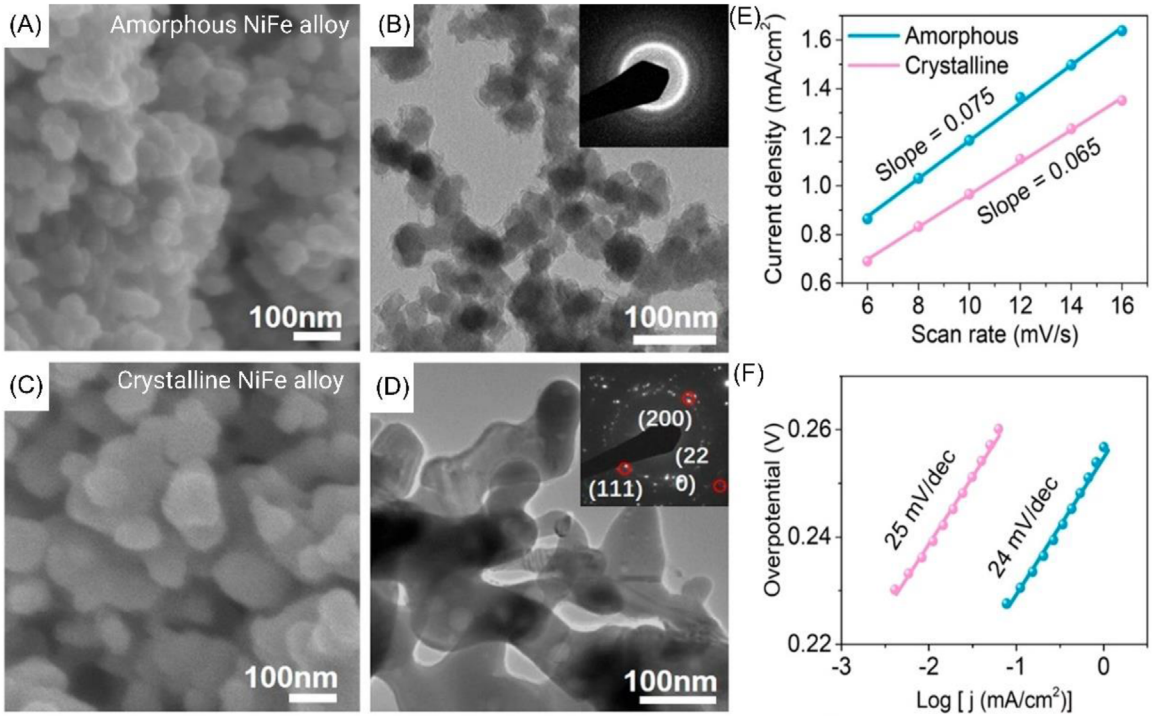

FIGURE 1 (A) Scanning electron microscopy (SEM) and (B) transmission electron microscopy (TEM) images of amorphous NiFe alloy catalyst. (C) SEM and (D) TEM images of crystalline NiFe alloy catalyst. Insets in (B) and (D) show the selected-area electron diffraction (SAED) patterns of amorphous and crystalline NiFe alloy catalysts, respectively. (E) Double-layer capacitances of amorphous and crystalline NiFe alloy catalysts to determine electrochemical active surface area (ECSA). (F) Tafel plots of amorphous (cyan) and crystalline (pink) NiFe alloy catalysts. *Source*: Reproduced with permission: Copyright 2020, American Chemical Society.[56]

3.1 | Flexible electronic structure

The long-range disorder feature gives rise to flexible electronic structures in amorphous TM-based catalysts, which results in two major advantages. Amorphous catalysts possess more defects or vacancies that are generally electroactive sites than long-range ordered crystalline counterparts.[58,59] As depicted in Figure 2A, the $LaNiO_3$ catalysts prepared at lower temperatures (450 and 500°C) possess a hybrid amorphous/crystalline feature, and the amorphous part shows no atomic periodicity.[60] This also leads to rich electronic properties, which can be identified by X-ray photoelectron spectra analysis. Compared with the crystalline NiO_x/NF-600°C catalyst, the Ni 2p3/2 spectrum of amorphous NiO_x/NF-100°C contains a higher ratio of high-valence Ni^{3+} species. In addition, the amorphous NiO_x/NF-100°C exhibits a higher concentration of oxygen defects. These favorable electronic features benefit the adsorption/desorption of reactants during UOR.[61] Accordingly, the flexible electronic structure of amorphous catalysts contributes to more catalytically active sites for ESM.

It is facile to introduce foreign metal/nonmetal elements into amorphous TM-based catalysts. Component regulation usually leads to bond length regulation and electron/charge redistribution,[62] which further optimizes the adsorption/desorption of reaction intermediates and benefits the catalysis process.[63,64] From the crystal models in Figure 2B,C, it can be observed that the atom arrangement of amorphous Fe-doped $InPO_4$ is disordered compared to the crystal counterpart. Further investigations suggest that the average Fe–O bond length (1.891 Å) in the amorphous Fe-doped $InPO_4$ is shorter than that of the crystalline one (1.913 Å) (Figure 2D). A shorter Fe–O bond distance would attribute to more high-valence Fe species and improve the interaction with catalytic intermediates.[44]

3.2 | Facile structure self-reconstruction

TM-based catalysts would undergo in situ structure reconstruction during electrochemical oxidation processes (e.g., OER, UOR, and GOR), resulting in the formation of stable and catalytically active TM (oxy)hydroxide species.[65] Compared with crystalline catalysts, amorphous TM catalysts could easier transform into active TM (oxy)hydroxides and achieve higher catalytic activities.[66,67] For example, Chen

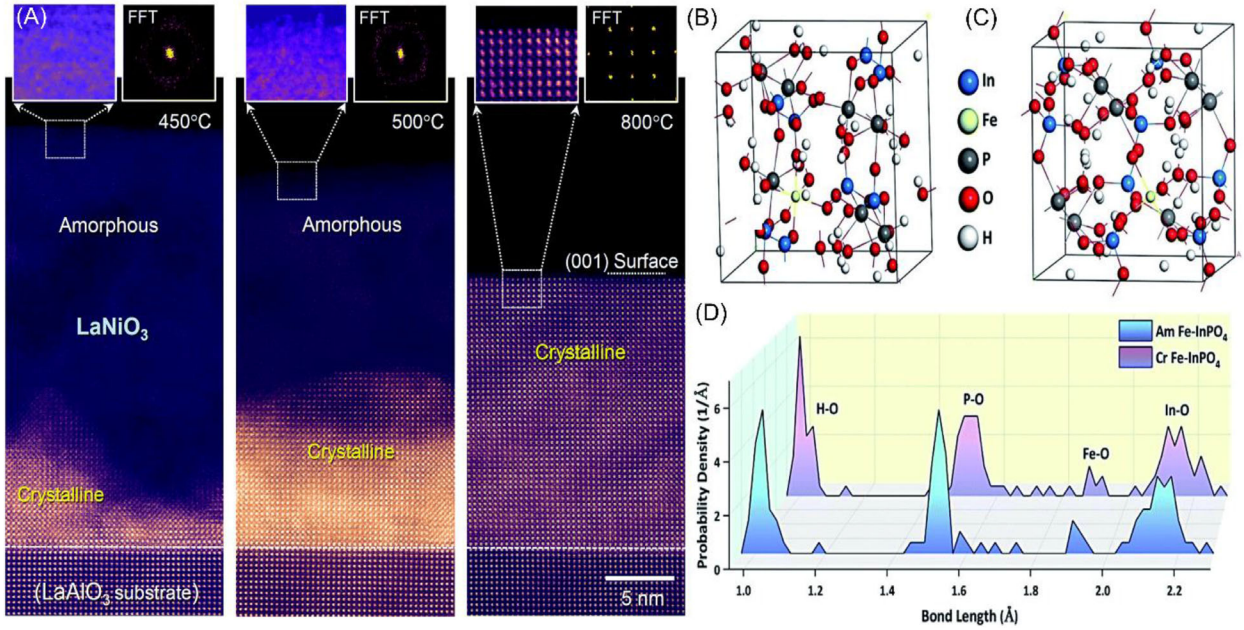

FIGURE 2 (A) Scanning transmission electron microscopy (STEM) images along with fast Fourier transforms (FFTs) clarify the surface regions in the $LaNiO_3$ catalyst annealed at 450, 500, and 800°C. Classical models of (B) amorphous Fe–$InPO_4$ and (C) crystalline Fe–$InPO_4$. (D) Distributions of average bond lengths in amorphous Fe–$InPO_4$ and crystalline Fe–$InPO_4$. *Source*: (A) Reproduced with permission: Copyright 2022, Royal Society of Chemistry.[60] (B–D) Reproduced with permission: Copyright 2020, Royal Society of Chemistry.[44]

et al. have compared the OER performance of the manually milled chalcopyrite ($CuFeS_2$-HM, crystalline phase) and the mechanically milled counterpart ($CuFeS_2$-BM, amorphous phase). The rich defects in $CuFeS_2$-BM lead to a flexible structure and can decrease the necessary energy for the self-formation of electroactive phases.[68] Such structure characteristics of $CuFeS_2$-BM promote the totally in situ evolution of the original sulfides into metal (oxy)hydroxide phases during OER, whereas electroactive phases/species in the $CuFeS_2$-HM catalyst are just confined on the shell/surface (Figure 3A).

Recent studies have taken the advantage of amorphous catalysts' facile structure self-reconstruction feature to design efficient electrocatalysts for ESM.[69,70] In the crystalline NiO/amorphous CrO_x heterostructure, the presence of amorphous CrO_x can facilitate the self-reconstruction of NiO to the active NiOOH phase and improve adsorption strength toward urea molecules, as evidenced by the in situ electrochemical Raman analysis.[28] The NiO/CrO_x catalyst thus shows good UOR performance, and a potential of 1.32 V is acquired to achieve the 10 mA cm^{-2} with long stability for 5 days. Similarly, a recent report suggests that amorphous Fe-doped NiB (aFe-NiB) needs lower energy (1.40 V vs. reversible hydrogen electrode [RHE]) than the crystalline counterpart (1.45 V vs. RHE) to initiate the structure reconstruction during the UOR process, as illustrated by the in situ Raman spectra (Figure 3B,C).[66] The aFe-NiB thus exhibits higher UOR performance due to the improved formation of electroactive metal oxyhydroxides.

4 | AMORPHOUS TM ALLOYS

Amorphous TM alloys are highly efficient ESM catalysts due to their high conductivity and the synergistic combination of electroactive metals, as well as rich active sites.[24,71] Co, Ni, and Fe-based amorphous alloys are widely explored ESM electrocatalysts, and current studies mainly focus on nanostructure design and heterostructure construction.

4.1 | Nanostructure design

Controlling the nanostructure of nanocatalysts is a powerful strategy to upgrade the catalytic performance of amorphous TM alloys by providing a large surface area and promoting the penetration/diffusion of electrolytes.[72,73] Porous materials,[74] nanoarrays,[75] pompoms,[19] films,[76] and aerogels[23] have been investigated for ESM. For instance, Xu et al. used electrodeposition to load amorphous NiFe nanotubes onto the nickel foam (NiFe NTAs-NF) (Figure 4A).[75] As shown in Figure 4B, the nanotube array nanostructures are presented. The well-defined nanotube arrays offer a large surface area, rich electroactive sites, as well as adequate electrolyte/gas transportation channels during the electrochemical reaction. Together with the amorphous phase of the NiFe alloy, the NiFe NTAs-NF exhibits a high OER activity (η_{50} = 216 mV) and good stability for 20 h. Similarly, the amorphous Ni–Co alloy/NF catalyst prepared by a three-step process shows a three-dimensional (3D) hierarchical nanorod array

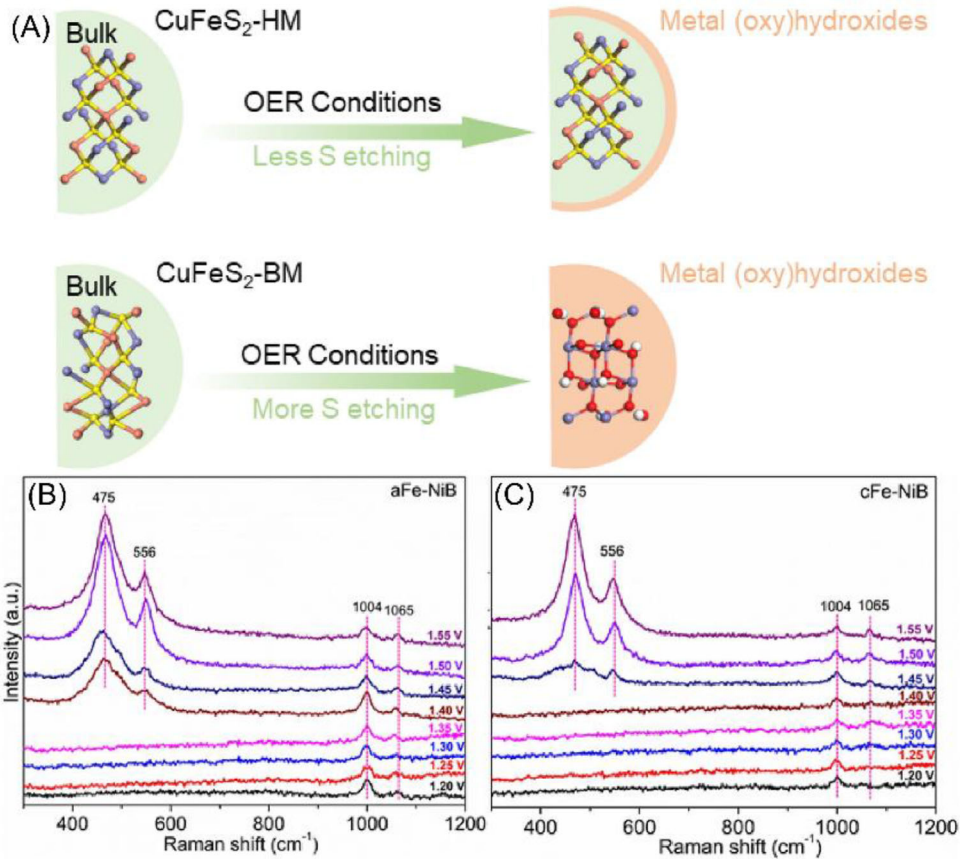

FIGURE 3 (A) Illustration of the in situ structure reconstruction of $CuFeS_2$-HM and $CuFeS_2$-BM during oxygen evolution reaction (OER) (color: white-H, yellow-S, red-O, brown-Cu, blue-Fe). In situ Raman spectra collected on (B) amorphous Fe-doped NiB and (C) crystalline Fe-doped NiB for urea oxidation reaction (UOR). *Source*: (A) Reproduced with permission: Copyright 2022, Elsevier.[68] (B and C) Reproduced with permission: Copyright 2023, Elsevier.[66]

nanostructure (Figure 4C,D).[77] Compared with the Ni/NF and Co/NF catalysts, the amorphous Ni–Co/NF catalyst shows better performance toward HzOR and attains a higher current density of 1213 mA cm^{-2} at 0.30 V versus RHE with good stability for 36 h (Figure 4E,F). Besides nanoarray structure, porous structures also possess a large number of exposed electroactive sites for OER.[78] Typically, the 3D ordered macro-/mesoporous $Ni_{61}Co_{39}$ alloys with large surface area and distinctive structure show a good performance for OER (η_{10} = 241 mV).[74]

4.2 | Heterostructure construction

Besides nanostructure manipulation, constructing heterostructures is another universal strategy to enhance the ESM performance of amorphous TM alloys. Heterostructures can inherit the merits (e.g., high activity, good conductivity, large surface area, and good durability) of different components harmonically and, thereby, contribute to upgraded catalytic performance. Wang et al. developed an eco-friendly exfoliator to assemble amorphous thin layered NiFe alloy nanosheets on two-dimensional (2D) materials (MoS_2, Ti_3C_2 MXene, graphene).[24] Taking the NiFe/MoS_2 as an example, the unique 2D/2D configuration largely limits the aggregation and improves the exposure of electroactive sites, and the strong interfacial coupling between MoS_2 and NiFe promotes charge transfer between them. Thus, the NiFe/MoS_2 heterostructure shows a high catalytic activity (η_{10} = 260 mV) for OER. Currently, the application of amorphous TM alloys in ESM is still in its infancy, and more studies are encouraged to regulate the physicochemical properties (e.g., porosity, size, conductivity, chemical composition, and shape) of TM alloys to upgrade their catalytic performance.

5 | AMORPHOUS TM (HYDR)OXIDES

TM (hydr)oxides are the most widely explored ESM catalysts owing to their easy preparation, high electrochemical activity, and eco-friendliness.[79,80] Amorphous TM (hydr)oxides with flexible crystal structures have exhibited good catalytic performance for ESM, especially Ni, Fe,

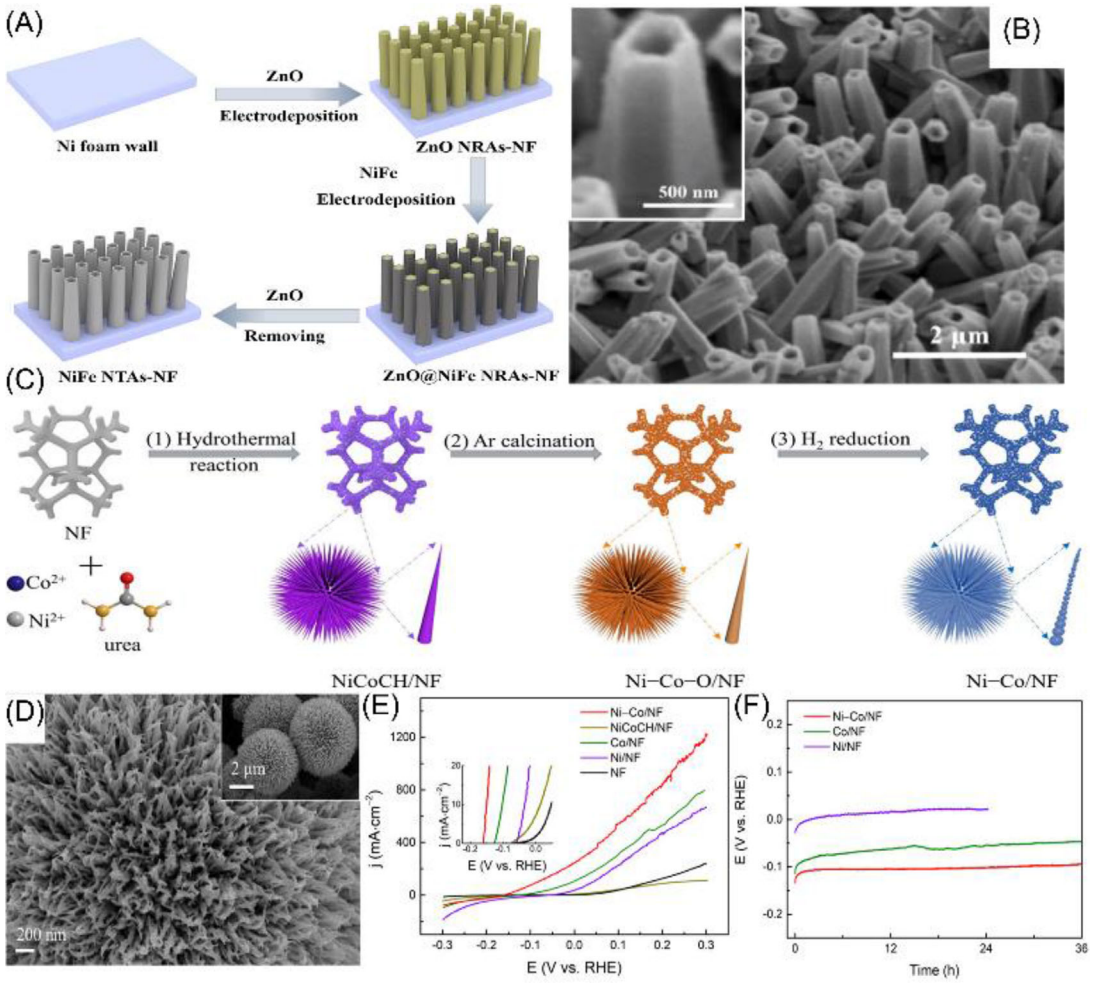

FIGURE 4 (A) Scheme of the fabrication of the NiFe NTAs-NF. (B) Scanning electron microscopy (SEM) image of NiFe NTAs-NF, the inset shows the single NiFe nanotube. (C) Scheme of the synthesis of amorphous Ni–Co/NF catalyst. (D) SEM image of the Ni–Co/NF catalyst. (E) Linear sweep voltammetry (LSV) curves of catalysts in 1 M NaOH + 0.5 M $N_2H_4 \cdot H_2O$ electrolyte. (F) Chronopotentiometry curves of catalysts at 10 mA cm^{-2}. *Source*: (A and B) Reproduced with permission: Copyright 2018, American Chemical Society.[75] (C–F) Reproduced with permission: Copyright 2020, American Chemical Society.[77]

Mn, and Co-based materials. Recently studies have provided great guidelines for the design of amorphous TM (hydr)oxides-based ESM catalysts.

5.1 | TM oxides

With high redox activity, flexible composition, and strong stability, amorphous TM oxides have aroused great interest in ESM catalysts.[81] Previous achievements suggest two general methods to enhance the catalytic performance of amorphous TM oxides, namely, component regulation, foreign-atom doping, and heterostructure construction.

5.1.1 | Component regulation

Compared with single metal oxides, binary/ternary/quaternary metal oxides with multimetallic active sites and rich redox couples gain growing attention.[82–84] A general rule for achieving a high ESM activity is combining more metal species in metal oxides. CoO_x is claimed to be more active than FeO_x and NiO_x, but the presence of a second metal (e.g., Ni, Ce, and Fe) can improve the OER performance of amorphous CoO_x significantly.[85] For instance, Pan et al. found that the amorphous Co–Ce oxides ($Co_{0.9}Ce_{0.1}O_x$) synthesized by a photochemical metal–organic deposition route show a good OER activity (η_{10} = 320 mV).[82] The presence of Ce can significantly improve the catalytic activity of CoO_x because of the synergistic effects of suitable metal–OH bond strength, enlarged SSA, and a high Co^{3+} proportion. Similar amorphous binary metal oxides such as Fe–Co oxides,[85] Fe–Ni oxides,[86,87] $NiWO_4$ nanoparticles,[88] and Ni–Co oxides[89] also have been investigated for ESM applications.

To further mediate the multi-electron transfer ESM process, oxides with multiple redox-active metal ion sites are

studied. Typically, Fe–Ni–Co oxides that have increased conductivity, populated catalytically active sites, and synergistic action of different elements present as highly efficient catalysts for ESM.[83,90] Aside from the activity, the addition of high-valence state Mo would upgrade Co–Fe oxides' stability.[91] In the amorphous quaternary Ba–Sr–Co–Fe oxide, the presence of abundant coordinately unsaturated active metal sites and the isotropic nature of amorphous oxides contribute to high OER performance.[92]

5.1.2 | Heteroatom doping

Foreign-atom doping is a universal strategy to adjust the physical/electronic properties of materials.[62] Both cationic and anionic dopings have been performed to optimize the ESM performance of amorphous oxides. Cationic doping generally can improve the charge transfer process, increase ECSA, and optimize the electronic structure of electroactive sites.[93] In an Fe-doped amorphous CoO_x, the Fe dopants not only provide active Fe sites to regulate the adsorption/desorption of OER intermediates but also tune neighboring Co sites' electronic structure to increase the OER performance.[26] A more recent investigation uncovers that the Mo dopant in $NiCo_2O_4$ leads to an amorphous and porous hierarchical structure and, thereby, contributes to high OER performance (η_{10} = 280 mV).[94] Moreover, the Mo-doped $NiCo_2O_4$ features a deep in situ reconstruction process under OER conditions and thus shows good performance durability for 24 h. With a higher electronegativity, Mo dopant in amorphous $MoCo_xO_y$ also can promote the participation of lattice oxygen in OER. The amorphous $MoCo_xO_y$ was prepared by a two-step process (Figure 5A).[95] Compared with the crystalline Co_3O_4 catalyst, oxygen vacancies can be witnessed on the amorphous $MoCo_xO_y$-100 catalyst (Figure 5B), suggesting the presence of high-energy dangling bonds. Electrochemical tests imply that the $MoCo_xO_y$-100 catalyst exhibits a strong pH-dependent OER activity, whereas Co_3O_4 shows a mostly pH-independent OER activity (Figure 5C). The pH-dependent OER activity result suggests a lattice oxygen oxidation mechanism (LOM) on the $MoCo_xO_y$-100 catalyst. Moreover, tetramethylammonium cation was introduced as a chemical probe to track the existence of superoxo-like (O^{2-}) and peroxo-like (O_2^{2-}) species that are typical intermediates in LOM-involved OER process. As shown in Figure 5D, the OER performance of $MoCo_xO_y$-100 is severely lessened in the presence of tetramethylammonium hydroxide (TMAOH), which reveals the critical contribution of LOM (Figure 5E).

Anionic doping is also studied to design ESM catalysts, based on amorphous TM oxides. Similar to cationic doping, the addition of anionic dopants can enhance the oxides' activity by regulating the amorphous property and the electronic structure of active sites. In a spinel $CuCo_2O_4$ catalyst, the P dopant induces the formation of the amorphous phase that provides rich active sites for OER.[96] The dual anion (N, S)-doping into the amorphous Ni–Co oxide can accelerate the catalytic kinetics by an "ensemble effect," which causes the electron distribution rearrangement. As a result, electrons in active metal centers are migrated into heteroatom, and thus, Co and Ni sites show higher oxidation states for OER.[97]

5.1.3 | Heterostructure construction

Integrating amorphous metal oxides with carbon materials or electroactive materials can enlarge ECSA, populate active sites, and enhance the intrinsic catalytic activity, thereby leading to upgraded catalytic performance.[98,99] Loading amorphous $Co_{0.6}Ni_{0.4}Fe_2O_4$ on N-doped carbon nanocubes can contribute to a high activity toward methane oxidation. The oxide/carbon hybrid generates methanol with a high selectivity of 82.8% and a yield of 1925.4 mmol $g_{cat.}^{-1}$ h^{-1} at 0.8 V versus Ag/AgCl.[100] Such catalytic performance originates from the robust trimetal–carbon electronic interaction and a high ratio of lattice oxygen/oxygen vacancy of the $Co_{0.6}Ni_{0.4}Fe_2O_4$/N-doped carbon nanocubes. Apart from carbon materials, construction composites by coupling amorphous oxides with crystalline active materials have been well demonstrated.[27,101] Qiao et al. developed a crystalline $CoNiP_x$/amorphous P-MnO_y (c-$CoNiP_x$/a-P-MnO_y) composite for UOR via a hydrothermal treatment-phosphization process (Figure 6A,B). The c-$CoNiP_x$/a-P-MnO_y catalyst can achieve the current density of 100 mA cm^{-2} at 1.35 V versus RHE for UOR, which is 273 mV lower than that for OER (Figure 6C). In addition, the composite outperforms the single component (Figure 6D,E), indicating the synergistic effect between the crystalline $CoNiP_x$ and amorphous P-MnO_y.[102] In the amorphous CrO_x confined Ni/NiO nanoparticles catalyst synthesized by a hydrothermal treatment-hydrogenation method (Figure 6F), the amorphous CrO_x can facilitate the in situ generation of active NiOOH phase and the electron transfer process during UOR (Figure 6G), contributing to high catalytic activities. Additionally, the CrO_x shell shows a protective effect and leads to high stability.[103]

5.2 | TM (oxy)hydroxides

TM (oxy)hydroxides are the most stable catalysts for ESM in neutral to alkaline media, and Ni/Fe/Co-based (oxy)hydroxides are excellent electrocatalysts.[104–106]

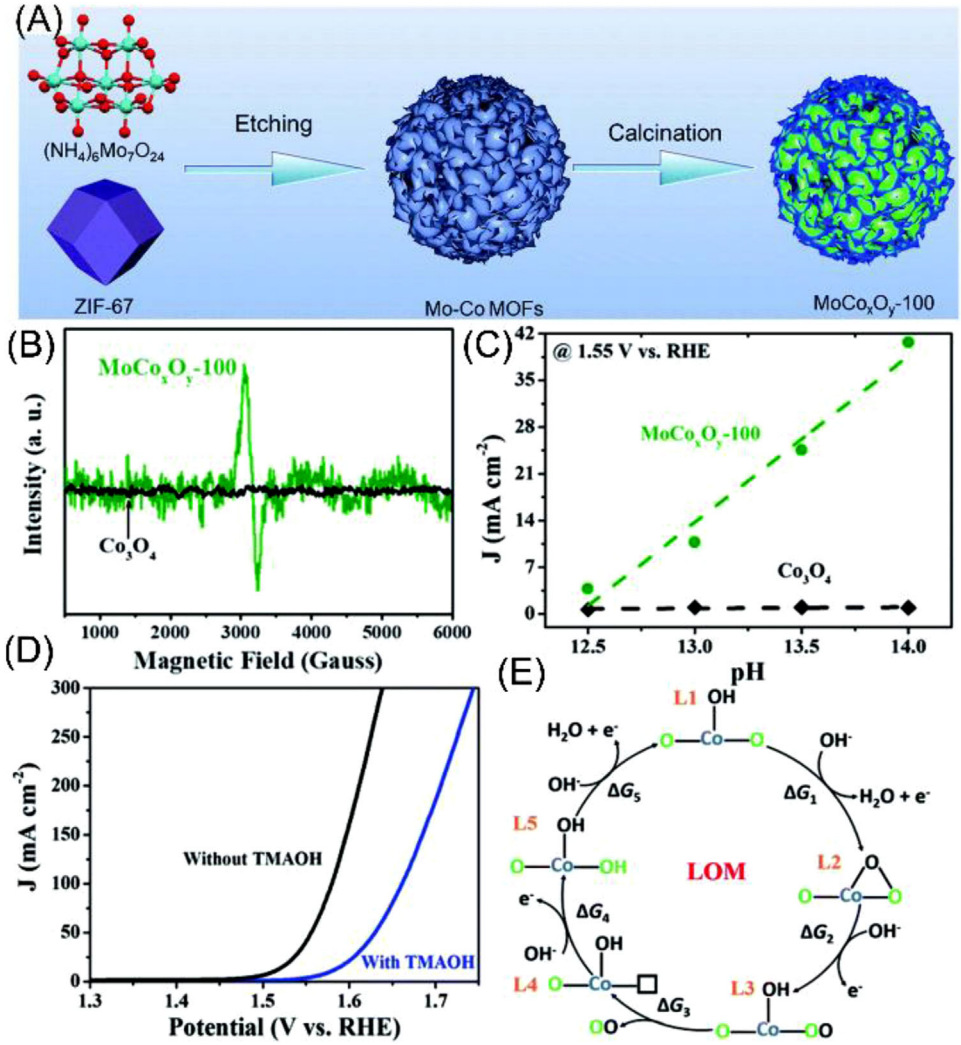

FIGURE 5 (A) Illustration of the synthesis of the amorphous $MoCo_xO_y$ catalyst. (B) Electron paramagnetic resonance (EPR) spectra of Co_3O_4 and $MoCo_xO_y$-100. (C) Current densities of Co_3O_4 and $MoCo_xO_y$-100 at 1.5 V versus RHE, as a function of pH value. (D) Linear sweep voltammetry (LSV) curves of $MoCo_xO_y$-100 in 1 M KOH with and without TMAOH. (E) Proposed lattice oxygen oxidation mechanism (LOM)-involved oxygen evolution reaction (OER) mechanism, where □ means the oxygen vacancy. *Source*: Reproduced with permission: Copyright 2022, Royal Society of Chemistry.[95]

For the development of high-performance amorphous (oxy)hydroxides, nanostructure design and heterostructure construction are two powerful methods.

5.2.1 | Nanostructure design

TM (oxy)hydroxides with different dimensions have been prepared and used as ESM catalysts. The amorphous zero-dimensional (0D) $Ni_{70}Fe_{30}$-(oxy)hydroxide synthesized by a sonochemical method possesses a small particle size of 2–3 nm, which contributes to high OER activities (η_{10} = 292 mV, Tafel slope = 30.4 mV dec^{-1}).[107] Starting from Fe-based bimetallic MIL-88 metal–organic frameworks (MOFs), Xu et al. developed amorphous bimetallic hydroxides via an in situ chemical transformation process.[108] The MOF-derived NiFe–OH-0.75 catalyst with ultrasmall nanoparticles (<10 nm) and abundant catalytically active sites only takes the overpotential of 270 mV to gain 10 mA cm^{-2}. 2D nanosheets are the most general structure of TM (oxy)hydroxides, which attract great interest.[109–111] For example, the porous amorphous nickel–iron hydroxide ($NiFe(OH)_2$) nanosheets with multi-metal coordination and highly porous nanostructure exhibit high HzOR activities (j = 10 mA cm^{-2}@0.06 V vs. RHE) and long-term stability (>22 h).[109] Amorphous nano/microarrays, nanocages, and nanocubes of TM (oxy)hydroxides with unique structures and rich abundance are efficient ESM catalysts.[112–115] Interestingly, the amorphous Ni–Co hydroxide nanodendrite forests

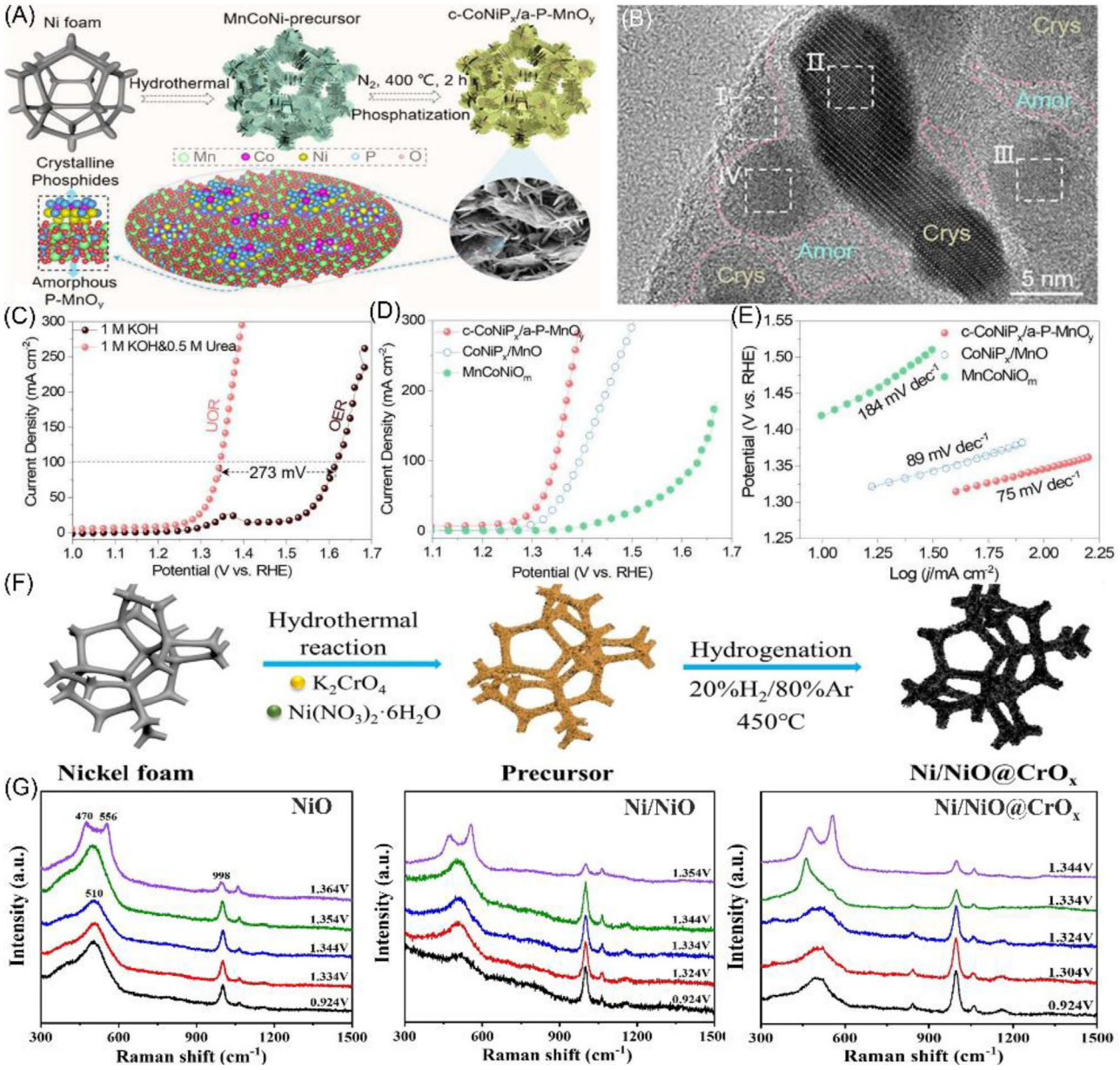

FIGURE 6 (A) Illustration of synthetic of c-CoNiP$_x$/a-P-MnO$_y$. (B) Transmission electron microscopy (TEM) image of c-CoNiP$_x$/a-P-MnO$_y$. (C) Linear sweep voltammetry (LSV) curves for oxygen evolution reaction (OER) and urea oxidation reaction (UOR) of c-CoNiP$_x$/a-P-MnO$_y$. (D) LSV curves and (E) Tafel plots of different catalysts. (F) Scheme of the preparation process of the Ni/NiO@CrO$_x$. (G) In situ electrochemical Raman spectra of NiO, Ni/NiO, and Ni/NiO@CrO$_x$ catalysts. *Source*: (A–E) Reproduced with permission: Copyright 2023, Elsevier.[102] (F and G) Reproduced with permission: Copyright 2023, Elsevier.[103]

developed by Balram et al. feature hierarchical nature, superhydrophilic property, and underwater superaerophobic behavior, which leads to high catalytic performance.[115] This study emphasized that the bubble generation and detachment behavior during the gas-involved reactions would affect the catalytic performance.

5.2.2 | Heterostructure construction

Constructing amorphous TM (oxy)hydroxides on the surface of electroactive and highly conductive materials (e.g., TMSs and TMPs) can contribute to high catalytic performance. There are generally two ways to form the amorphous TM (oxy)hydroxides-based heterostructures, pre-synthesis route, and in situ electrochemical reconstruction. The pre-synthesis route means that amorphous TM (oxy)hydroxides are formed during the catalyst synthesis process via electrodeposition,[116] precipitation,[13,117] chemical deposition,[29] and so on. For instance, Lv et al. prepared crystalline NiFe/amorphous NiFe-(oxy)hydroxide on the NiMo alloy (NM@cNF/aNFO) by electrodeposition, as illustrated in Figure 7A.[118] The abundant nanopores and defects of amorphous NiFe-(oxy)hydroxide, the high

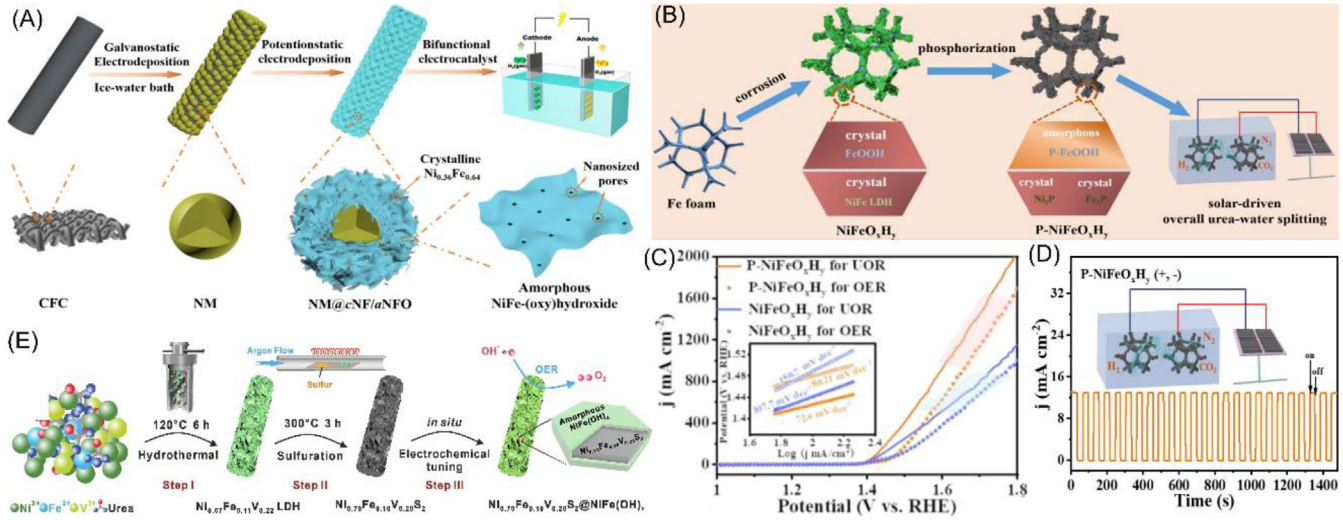

FIGURE 7 (A) Scheme of the synthesis of crystalline NiFe/amorphous NiFe-(oxy)hydroxide on NiMo alloy. (B) Illustration of the synthesis of P-$NiFeO_xH_y$ electrocatalyst. (C) Linear sweep voltammetry (LSV) curves of P-$NiFeO_xH_y$ and $NiFeO_xH_y$ for oxygen evolution reaction (OER) and urea oxidation reaction (UOR), the inset is the corresponding Tafel plots. (D) *j–t* curve under chopped illumination, the inset is the schematic diagram of the simulated solar-driven urea electrolysis system. (E) Schematic of the preparation of the $Ni_{0.70}Fe_{0.10}V_{0.20}S_2$@amorphous NiFe hydroxide catalyst. *Source*: (A) Reproduced with permission: Copyright 2022, Elsevier.[118] (B–D) Reproduced with permission: Copyright 2023, Elsevier.[120] (E) Reproduced with permission: Copyright 2022, Elsevier.[125]

electronic conductivity and rich edges of ultrafine NiFe nanocrystals, and the tight combination of NiMo alloy toward the outer nanosheets lead to abundant electroactive sites, high intrinsic activity, fast mass/charge transfer, and high electrocatalytic durability. Similar studies also integrate the advantages of amorphous TM (oxy)hydroxides with other electroactive materials to gain cost-effective ESM catalysts, such as $Ni(OH)_2$/amorphous $Cu(OH)_2$,[13] amorphous Fe hydroxides/V-doped nickel sulfide,[29] amorphous $NiFe(OH)_x/(Ni, Fe)Se_2$,[119] Ni–Fe–OH@Ni_3S_2/NF,[117] and amorphous NiFe–OH/NiFeP.[116] It is interesting to find that some of the amorphous hydroxide-based composites exhibit high performance toward multiple reactions, which is favorable for system simplification. Li et al. developed a crystalline NiFe phosphide/amorphous P-doped FeOOH hybrid (P-$NiFeO_xH_y$) for UOR, OER, and HER via a corrosion-phosphorization method (Figure 7B).[120] Compared with the crystalline $NiFeO_xH_y$ catalyst, P-$NiFeO_xH_y$ exhibits better performance toward OER and UOR (Figure 7C) due to its ameliorated adsorption energy of oxygen-containing reactants and superaerophobic and superhydrophilic surface. The P-$NiFeO_xH_y$ catalyst can be implemented as both anode and cathode for the urea electrolyzer, which can achieve 10 mA cm^{-2} at a voltage of 1.36 V and could be driven by a solar cell system (Figure 7D).

In alkaline electrolytes, the in situ electrochemical reconstruction mediated TM (oxy) hydroxide formation has been well accepted in the last few years.[121,122] It is suggested that most TM-based catalysts will undergo structure reconstruction and generate (oxy)hydroxides on the catalysts' surface, under alkaline and oxidative conditions.[68,123,124] With this in mind, many studies have focused on the in situ electrochemical construction of high-performance heterostructures for ESM. Yang et al. designed an $Ni_{0.70}Fe_{0.10}V_{0.20}S_2$@amorphous NiFe hydroxide catalyst for OER by thermal sulfidation and a subsequent in situ electrochemical treatment (Figure 7E).[125] The high electronic conductivity of the inner $Ni_{0.70}Fe_{0.10}V_{0.20}S_2$, synergistic effects between NiFe hydroxides and $Ni_{0.70}Fe_{0.10}V_{0.20}S_2$, and stable electroactive sites on the outer amorphous hydroxide surface together benefit the OER performance (η_{10} = 204 mV). In contrast to the pre-synthesis strategy, the inevitable in situ electrochemical conversion process is more convenient and practical for designing TM-based heterostructural catalysts for ESM.

6 | AMORPHOUS TM CHALCOGENIDES

TM chalcogenides (sulfides, selenides, and tellurides) as emerging (pre)catalysts with excellent ESM performance have gained growing scientific attention owing to their high electrical conductivity, good catalytic activity, as well as low cost.[126,127] Typically, amorphous TM chalcogenides with rich defects, dangling bonds, and structural flexibility are highly promising ESM (pre)catalysts. In this section, the recent advances in the development of

amorphous TM chalcogenides (sulfides, selenides) for ESM are detailed.

6.1 | TM sulfides

Amorphous TM sulfides have been extensively used for ESM, especially bimetallic sulfides.[128] Designing amorphous TM sulfides for ESM generally involves the modification of materials' internal and external characteristics, including morphology/nanostructure, electrical conductivity, and electronic structure.[129] To achieve these goals, nanostructure design, heteroatom doping, and heterostructure construction have been extensively studied.

6.1.1 | Nanostructure design

To populate the electroactive sites and fasten charge/mass transfer, controlling the nanostructure of amorphous TM sulfides is an efficient method. 2D amorphous TM sulfide nanosheets[130–132] and nanoflake arrays[133] are representative catalysts. To avoid the formation of dense structures or films, engineering holes/pores on the sulfide nanosheets can enlarge the surface area of catalysts and promote the release of generated oxygen gas bubbles.[132,134] For instance, the honeycomb-like amorphous Ni–Mo–S membrane composed of abundant intertwined ultrathin nanosheets can realize a current density of 100 mA cm^{-2} at 1.385 V for UOR.[135] Improving the dispersion of electroactive sites via nanostructure design also contributes to high catalytic performance. Dong et al. prepared highly dispersed amorphous cobalt/nickel sulfides with a nanoflakes array structure by controlling the synthetic conditions.[133] The optimal amorphous Co_4Ni_1S nanoflake arrays exhibit good OER and HER activities, and it takes a low cell voltage (1.60 V) to attain 10 mA cm^{-2}, with high stability (96% activity retention for about 10 h).

6.1.2 | Heteroatom doping

Aside from structure regulation, raising the intrinsic activity of amorphous TM sulfides via heteroatom doping is suggested. In 2017, Cai et al. developed oxygen-doped amorphous cobalt sulfide porous nanocubes for OER.[136] The oxygen dopants lead to desirable reaction intermediate (O*) adsorption energy and distorted $CoS_{4.6}O_{0.6}$ octahedron structure, which synergistically contributes to improved OER activities (η_{10} = 290 mV). More recently, ultrathin and amorphous Mo-doped FeS nanosheets with abundant sulfur defects were developed via a hydrothermal route.[137] Benefited from the amorphous ultrathin nanosheets structure and synergistic effects of Mo dopants and S defects, the Mo-doped FeS manifests good OER activities (η_{10} = 210 mV, Tafel slope = 50 mV dec^{-1}) and stability in the alkaline medium.

6.1.3 | Heterostructure construction

Hybridizing amorphous TM sulfides with electroactive nanomaterials (e.g., oxides, metal particles, sulfides, hydroxides, and tellurides) and highly conductive carbon materials can further upgrade the catalytic performance.[138–140] Liu et al. designed a bifunctional catalyst composed of Cu cluster-coupled quasi-amorphous on Cu foam (CF) CoS_x (Cu@CoS_x/CF) via a one-step route (Figure 8A).[141] With the CF support, the Cu@CoS_x/CF is somewhat flexible (Figure 8B), and the Cu@CoS_x/CF manifests a 3D macroporous structure (Figure 8C). These structural features benefit the exposure of active sites, charge/mass transfer, and mechanical stability. In addition, Cu clusters have multiple effects on the catalytic performance of Cu@CoS_x/CF. First, the Cu cluster could improve the electronic transport property of the Cu@CoS_x/CF hybrid. Second, the Cu cluster could interact with quasi-amorphous CoS_x strongly at the interface, which leads to the generation of rich negative and positive sites and further promotes the interaction of the catalyst with H_2O. Third, Cu clusters can benefit H_2O dissociation and facilitate the electrolyzing of water. With these merits, the Cu@CoS_x/CF//Cu@CoS_x/CF couple can afford 10 mA cm^{-2} at about 1.50 V in an alkaline electrolyzer.

Compositing amorphous TM sulfides with (hydr)oxides/sulfides/tellurides also contributes to high catalytic performance. For example, the NF-supported hierarchical OER catalyst (VO_x/Ni_3S_2@NF) comprising vanadium oxide nanocrystals (VO_x) embedded in amorphous nickel sulfide (Ni_3S_2) nanosheets can attain 100 mA cm^{-2} at a low overpotential (358 mV) (Figure 8D).[142] Apart from the self-supported hierarchical nanostructure and the rational chemical composition, the presence of VO_x in the sulfide nanosheets upgrades the catalytic performance by strengthening the Ni–O bonds. Amorphous TM sulfides/chalcogenides heterostructures which gather the advantages of different sulfides and benefit from the synergistic effect among different components also present high ESM activities, such as MoS_x@Co_9S_8@Ni_3S_2/NF,[139] Ni_3S_2/MoS_x nanosheets/NF,[143] NiTe/amorphous NiS,[34] Mn–Cd–S@amorphous-Ni_3S_2,[144] amorphous MoS_2/CoS/$Co_{0.85}Se$ nanotube arrays,[35] and a-MoS_2–Ni_3S_2/NF.[145]

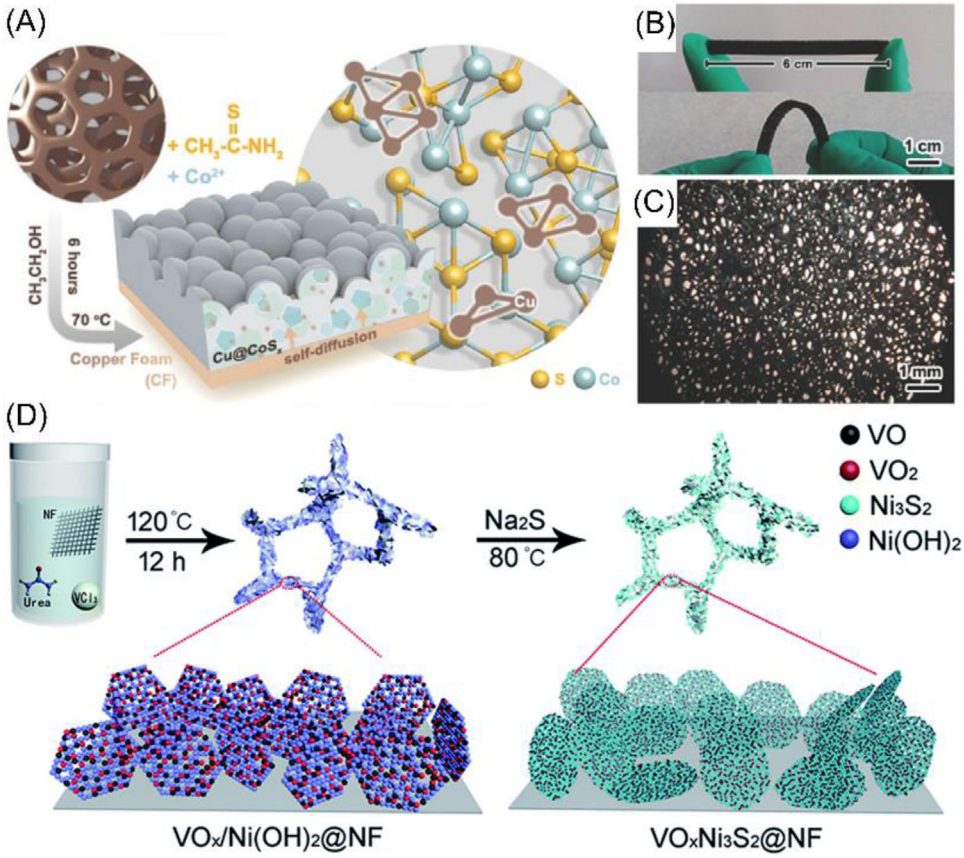

FIGURE 8 (A) Scheme of the preparation of Cu@CoS_x/CF. (B and C) Digital images of Cu@CoS_x/CF. (D) Illustration of the synthesis of VO_x/Ni_3S_2@NF via a two-step hydrothermal route. *Source*: (A–C) Reproduced with permission: Copyright 2017, Wiley-VCH.[141] (D) Reproduced with permission: Copyright 2019, Royal Society of Chemistry.[142]

6.2 | TM selenides

Amorphous TM selenides such as Ni_xSe_y, Fe_xSe_y, and Co_xSe_y have attracted great attention as ESM catalysts for their high conductivity, metallic properties, and good electroactivity.[146,147] Binary metal selenides that combine different active metal species have exhibited better ESM performance than their monometallic counterparts. Yi et al. developed amorphous Ni–Fe–Se/NF hollow nanospheres for both HER and OER via electrodeposition.[36] The Ni–Fe–Se/NF outperforms the single metal counterparts for water splitting because of the synergistic effect of Fe and Ni.

Amorphous TM selenides-based composites such as Cu-doped amorphous $NiSe_x$/crystalline $NiSe_2$ (Cu-(a-$NiSe_x$/c-$NiSe_2$)/TiO_2),[37] amorphous Co–CoO_x/CoSe composite film,[148] amorphous MoS_2/CoS/$Co_{0.85}Se$ nanotube arrays,[35] and amorphous Co–O@Co–Se film[149] are high-performance ESM catalysts. Of note, the amorphous/crystalline heterostructure (Cu-(a-$NiSe_x$/c-$NiSe_2$)/TiO_2) developed by Park et al. possesses some meaningful characteristics.[37] First, the outer amorphous $NiSe_x$ phase can efficiently decrease the size of inner crystalline particles and stabilize them from aggregation, which contributes to a large surface area. Second, the rich defect sites of the amorphous $NiSe_x$ provide abundant electroactive centers, and the inner $NiSe_2$ structure's good electrical conductivity leads to a synergistic effect, thus enhancing the composite's catalytic activity and stability.

7 | AMORPHOUS TM PHOSPHIDES, NITRIDES, BORIDES, AND OXOMETALLATES

7.1 | TM phosphides and nitrides

TM phosphides and nitrides with metallic properties, high electrical conductivity, and good electrochemical activity are promising ESM catalysts. The design of high-performance amorphous TM phosphides and nitrides-based catalysts generally involves component regulation, nanostructure design, and heterostructure construction.

7.1.1 | Component regulation

The introduction of external metals or nonmetals can ameliorate the catalytic performance of single metal phosphides/nitrides. It has been well proved that amorphous NiFeCoP catalysts perform better than their mono/binary metallic counterparts.[150,151] The main reason is that the abundant electroactive sites, disordered atomic arrangements, and synergic effects of different metals contribute to enhanced catalytic activity. A general trend is that more metal species lead to higher ESM catalytic performance,[152–154] and the ratio of metals also plays a vital role.[40,155] Aside from the addition of metals, recent studies indicate that anions also can tune the catalytic behavior of amorphous TM phosphides. In a B-involved ternary Co–P catalyst, the Co–P–B could inherit great electron transfer properties from Co–B and Co–P. Hence, the addition of B can regulate the electron transfer process of the ternary catalyst.[156] In addition, the optimal Co–P–B-5 catalyst undergoes obvious structure reconstruction during anodic polarization and facilitates the generation of abundant CoOOH active species on its surface.

7.1.2 | Nanostructure design

Catalysts with large particle sizes and dense layer structures are less likely to expose enough electroactive sites for catalytic reactions. In this context, controlling the nanostructure of amorphous TM phosphides/nitrides is in high demand. Currently, amorphous TM phosphides/nitrides with various nanostructures like nanospheres,[157] hierarchical nanosheet arrays,[158] thin films,[159] nanosheets,[160,161] and nanocone arrays[162] have been designed for ESM. An efficient method to construct typical nanostructures is using a template. For example, Huang et al. employed a template-assisted strategy to construct carbon fiber paper-supported amorphous $CoMoP_x$ nanosheet arrays (a-$CoMoP_x$/CF) (Figure 9A).[158] In the synthetic process, Co-MOF and $CoMoO_4$ act as templates that ease the generation of amorphous $CoMoP_x$ by introducing abundant defects and dense voids. Benefiting from the hierarchical nanosheet arrays, amorphous structures, and the synergistic effect of Co/Mo components, the a-$CoMoP_x$/CF shows better activity than the noble metal-based counterparts for full water electrolysis. Employing the a-$CoMoP_x$/CF as the cathode and anode, a current density of 10 mA cm^{-2} can be attained at an applied cell potential of 1.581 V (Figure 9B,C), with good stability at 100 mA cm^{-2} for 100 h (Figure 9D). Another study used a ZnO template to develop O-incorporated NiMoP on NF (O-NiMoP/NF, Figure 9E), which shows nanotube array architecture with rich pores (Figure 9F).[163] The O-NiMoP/NF electrode shows good activities toward both UOR and HER, and using O-NiMoP/NF as the bifunctional electrode can realize energy-saving hydrogen production, as schematically in Figure 9G. Compared with the noble metal-based Pt/C/NF||RuO_2/NF couple, the O-NiMoP/NF electrodes attain a current density of 50 mA cm^{-2} with much lower energy consumption and a high hydrogen production FE of 96.8% (Figure 9H,I).

7.1.3 | Heterostructure construction

To simultaneously meet the multiple requirements of electrocatalysis, researchers have designed diverse heterostructures based on amorphous TM phosphides/nitrides. Generally, two types of composites are studied, the amorphous TM phosphides/nitrides-conductive carbon hybrids and amorphous TM phosphides/nitrides-electroactive materials hybrids. Loading amorphous TM phosphides/nitrides on highly conductive carbon materials can decrease particle aggregation and improve electrical conductivity.[41] Zou et al. coupled amorphous CoN_x nanoparticles within 3D N-doped graphene aerogel, and the nanohybrid with hierarchical porous structure and rich dual active sites (CoN_x and N_xC) shows high OER activities (η_{10} = 295 mV).[164] In 2020, Li et al. deposited amorphous NiFe phosphides on a 3D N-doped carbon paper (NCP), and the obtained NiFe-P/NCP OER electrode takes a relatively low overpotential of 226 mV to attain 50 mA cm^{-2}.[165] In these studies, anchoring electroactive species on 3D carbon materials benefits increased ECSA, electron transfer, and mass transportation and, thus, improves the catalytic performance. Interestingly, a recent study suggested that carbon materials can regulate the intrinsic catalytic of amorphous CoP.[166] The halogen (X = F, Cl, and Br)-doped carbon dots (CDs) modified amorphous CoP (X-CDs/CoP) was prepared via a two-step reaction of hydrothermal treatment and phosphorization (Figure 10A, F-CDs/CoP as an example). Compared with Cl or Br-doped CDs/CoP, the F-doped sample exhibits the best catalytic performance toward OER and HER (Figure 10B). With good HER and OER performance, the F-CDs/CoP can work as bifunctional catalysts for overall water splitting with high efficiency and good durability over 100 h (Figure 10C). In-depth density functional theory (DFT) calculations reveal that F-CDs/CoP exhibits lower energy barriers for both HER and OER than those of Cl or Br-doped CDs/CoP (Figure 10D,E), and the main reason is that the charge transfer between F-CDs and CoP is more prominent compared with the other X-CDs/CoP.

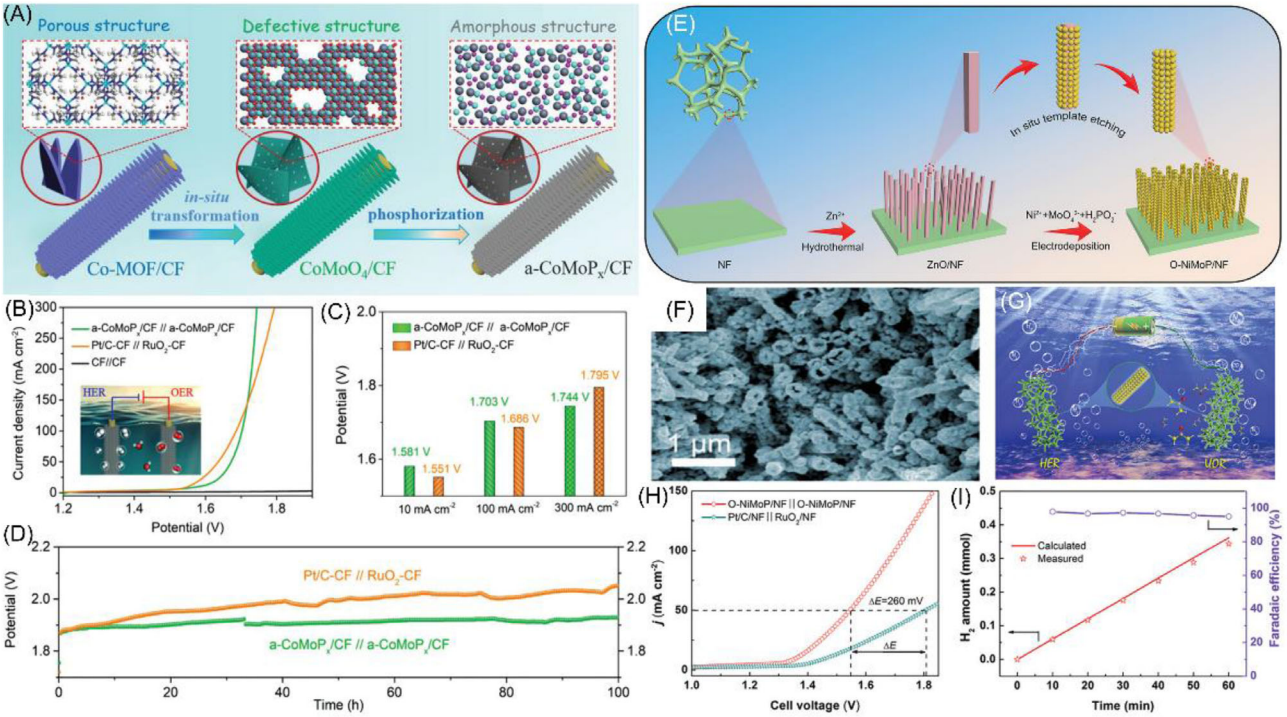

FIGURE 9 (A) Scheme of the template-assisted synthesis of a-$CoMoP_x$/CF. (B) Polarization curves of catalysts for full water electrolysis. (C) Required potentials for different catalysts to attain different current densities. (D) Stability curves for Pt/C-CF//RuO_2-CF and a-$CoMoP_x$/CF//a-$CoMoP_x$/CF at 100 mA cm^{-2}. (E) Scheme of the synthesis of O-NiMoP/NF. (F) Transmission electron microscopy (TEM) image of O-NiMoP nanotubes. (G) Scheme of the urea electrolysis system using O-NiMoP/NF as the bifunctional electrodes. (H) Linear sweep voltammetry (LSV) curves of Pt/C/NF||RuO_2/NF electrodes and O-NiMoP/NF couple in the urea electrolysis system. (I) FE of hydrogen production in urea electrolysis system within 1 h. Source: (A–D) Reproduced with permission: Copyright 2020, Wiley-VCH.[158] (E–I) Reproduced with permission: Copyright 2021, Wiley-VCH.[163]

Hybridizing amorphous TM phosphides/nitrides with other redox-active materials also gains great interest. Amorphous CoP_x-CoO_y composites,[167] NiOOH@amorphous Ni–P,[168] Ni@amorphous NiP/C,[38] mesoporous Ni_2P@$FePO_xH_y$,[169] and amorphous Co_2P@Co_2P/Co-polyoxometalate/NF[170] are some representative hybrids for ESM. In a triple-hierarchical porous Ni(Cu)@NiFeP/NF catalyst prepared by a two-step electrochemical process (Figure 10F), rich micropores and nanotubes can be well observed (Figure 10G,H).[39] The transmission electron microscopy image shows that the crystalline Ni(Cu) is tightly covered by amorphous NiFeP (Figure 10I). Such nanostructural, compositional, and crystalline/amorphous features offer abundant electroactive sites and shortened electron transfer pathways. Thus, the Ni(Cu)@NiFeP/NF catalyst outperforms single Ni(Cu), NiFeP, and even the Pt/C catalysts for HzOR (Figure 10J,K).

7.2 | TM borides

Amorphous TM borides are efficient ESM electrocatalysts, which feature facile preparation, high electrical conductivity, and high redox activity. Typically, the reverse electron transfer from B to TMs in amorphous TM borides results in enriched electrons on TMs and thus improves the electrocatalytic process.[72] To engineer high-performance amorphous TM borides for ESM, current efforts focus on nanostructure design, component regulation, heteroatom doping, and heterostructure construction.

7.2.1 | Nanostructure design

Amorphous TM borides are generally synthesized by a facile chemical reduction or electroless deposition process, with $NaBH_4$ or KBH_4 as the reductant and boron source.[171] The violent chemical reaction often leads to severe aggregation of boride particles, which limits the surface area of boride catalysts. To overcome this issue, researchers have developed a series of nanostructures by controlling the reaction conditions (e.g., temperature, time, reactants dosage, solvents, and precursors). For example, Li et al. synthesized one-dimensional (1D) NiCoFeB nanochains in the presence of polyvinyl pyrrolidone.[172] 2D amorphous TM borides nanosheets with high surface areas also have been designed, and studies of Nsanzimana et al.

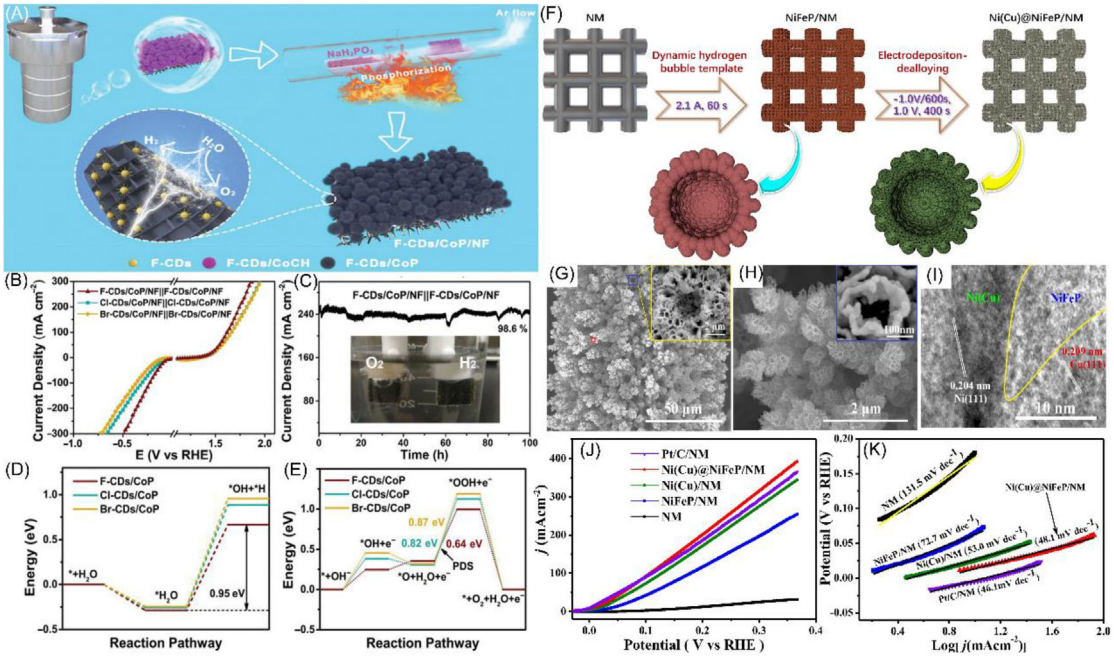

FIGURE 10 (A) Scheme of the synthesis of F-CDs/CoP/NF catalyst. (B) Two-electrode linear sweep voltammetry (LSV) curves of X-CDs/CoP/NF||X-CDs/CoP/NF for water electrolysis in 1 M KOH. (C) Chronoamperometric measurement of water electrolysis at 1.81 V, and the inset displays the F-CDs/CoP/NF||F-CDs/CoP/NF electrolyzer. Free-energy diagrams for (D) hydrogen evolution reaction (HER) and (E) oxygen evolution reaction (OER) on X-CDs/CoP (X = F, Cl, and Br) surfaces. (F) Illustration of the fabrication process of the hierarchical Ni(Cu)@NiFeP/NM composite on nickel mesh (NM). (G and H) SEM images of Ni(Cu)@NiFeP/NM. (I) Transmission electron microscopy (TEM) image of Ni(Cu)@NiFeP/NM. (J) Hydrazine oxidation reaction (HzOR) polarization curves of NM, Ni(Cu)/NM, Ni(Cu)/NM, NiFeP/NM, and Ni(Cu)@NiFeP/NM and (K) corresponding Tafel plots. CD, carbon dot. *Source*: (A–E) Reproduced with permission: Copyright 2022, Wiley-VCH.[166] (F–K) Reproduced with permission: Copyright 2019, Elsevier.[39]

suggest that CoB_x and Ni-FeB nanosheets with a higher surface area show better OER performance than nanoparticle counterparts.[173,174] What is more, the hierarchical structure of mixed metal FeNiCuSnBs guarantees efficient mass/charge transfer, sufficient electrochemical active sites, and rich transportation channels for electrolytes and produced oxygen gas.[175] Recent studies have innovated the design of hierarchically structured amorphous TM borides by using MOF as metal precursors.[176,177] By performing controllable boronization on the Co–Fe Prussian blue analog, Wang et al. successfully developed self-supporting CoFeB with rich electrochemical active sites and maintained nanocages-on-nanosheets structures.[178] The self-supporting boride electrode with multiple nanostructures gives rise to high OER performance (η_{10} = 255 mV, Tafel slope = 51 mV dec^{-1}).

7.2.2 | Component regulation

It is an efficient strategy to enhance amorphous TM borides' catalytic performance by chemical component regulation. Compared with monometallic borides (e.g., FeB, NiB, and CoB), binary and ternary metal borides with multimetallic active sites and multiple redox couples exhibit better performance.[179–181] In a binary CoFeB catalyst, the presence of Fe is suggested to stabilize Co species in the high-oxidation state and to accelerate the formation of OOH-like intermediates during OER.[182] It should be noted that more metal species in borides do not guarantee better OER activity. Cai et al. found that the addition of Mo in FeNiB can enhance the OER performance, whereas the presence of Mn reduces the catalytic activity of FeNiB.[183] In-depth analysis indicates that the incorporation of high-valent Mo^{6+} (low-valent Mn^{2+}) into NiFeB leads to decreased (increased) electron density near the Fermi level because of the high (low) electron affinity of Mo^{6+} (Mn^{2+}) and, thus, weakens (improves) the adsorption strength of oxygenated intermediate species. With regulated intermediates adsorption energies, the amorphous ternary NiFeMoB catalyst takes a low OER overpotential of 220 mV at 500 mA cm^{-2}. Incorporating anions into amorphous TM borides also can boost electrochemical performance. A representative is mixed metal–B–P catalysts, such as Ni–Fe–P–B[184] and Fe–Ni–P–B–O[185]. In the Ni–Fe–P–B catalyst, the unique amorphous structure and the metal-metalloid combined composition modulation give rise to a good OER activity (η_{10} = 269 mV).[184]

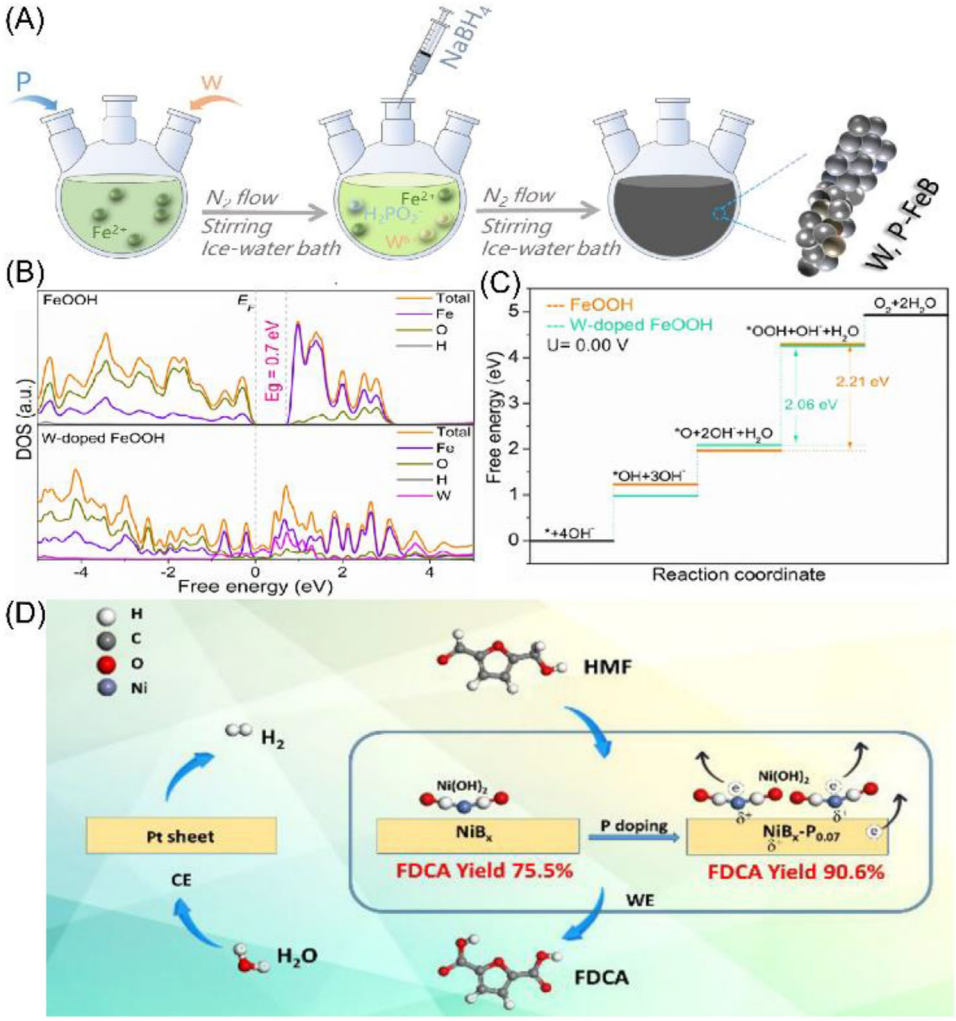

FIGURE 11 (A) Scheme of the synthesis of W, P co-doped FeB. (B) The computed density of state (DOS) for FeOOH and W-doped FeOOH. (C) Free-energy diagrams for oxygen evolution reaction (OER) on W-doped FeOOH and FeOOH at zero potential. (D) Illustration of the effect of P doping on the oxidation of 5-hydroxymethylfurfural (HMF). *Source*: (A–C) Reproduced with permission: Copyright 2021, Elsevier.[42] (D) Reproduced with permission: Copyright 2020, American Chemical Society.[21]

7.2.3 | Heteroatom doping

Heteroatom doping is a universal and favorable method to increase the catalytic activity of amorphous TM borides.[186] In a Ce-doped amorphous NiB catalyst, the synergistic effect of binary Ce and Ni metals contributes to high OER activity.[187] In addition, the self-evolution of the catalyst under the OER condition leads to the formation of CeO_{2-x} which acts as the electron acceptor and facilitates the generation of crystalline high-valent nickel species, leading to robust electrocatalysis. Besides cationic doping, Chen et al. developed an anion–cation dual doping method to boost OER properties of FeB. The W, P co-doped FeB catalyst was fabricated with a chemical reduction process (Figure 11A).[42] The W, P co-doped FeB catalyst presents a high OER activity in the alkaline electrolyte (η_{10} = 209 mV). It is disclosed that the anion (B and P) etching facilitates the evolution of FeOOH. Further DFT calculations indicate W dopants can boost the intrinsically catalytic activity by improving the conductivity (Figure 11B) and tuning adsorption/desorption energies of OER intermediates (Figure 11C). Another study has developed a P-doped NiB for the electrochemical oxidation of HMF. The P dopant leads to relative the displacement of electrons from the surface Ni and increased surface $Ni(OH)_2$ species, which increases the yield of FDCA from 75.5% of NiB to 90.6% (Figure 11D).[21]

7.2.4 | Heterostructure construction

Loading amorphous TM borides on conductive/large area substrates or electroactive materials to construct efficient heterostructures for ESM has been successfully

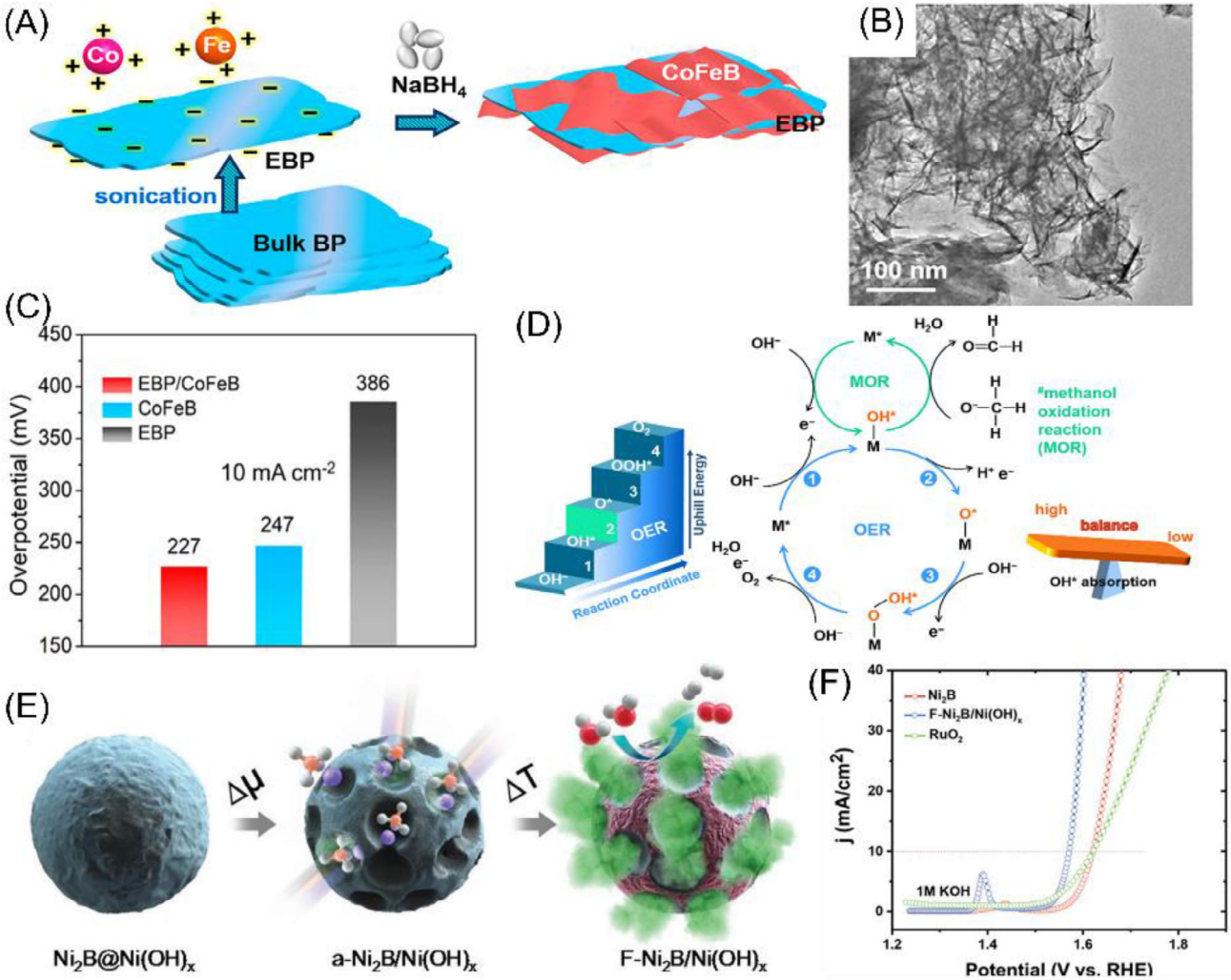

FIGURE 12 (A) Scheme of the synthesis of exfoliated black phosphorus (EBP)/CoFeB. (B) Transmission electron microscopy (TEM) image of EBP/CoFeB. (C) Overpotentials for oxygen evolution reaction (OER) at 10 mA cm^{-2}. (D) Scheme of the reaction processes for OER and MOR. (E) Scheme of the design process of F-Ni_2B/Ni$(OH)_x$. (F) Polarization curves of the F-Ni_2B/Ni$(OH)_x$, Ni_2B, and the RuO_2 catalyst. *Source*: (A–D) Reproduced with permission: Copyright 2021, American Chemical Society.[58] (E) Reproduced with permission: Copyright 2020, Wiley-VCH.[196]

implemented.[188] Substrates like reduced graphene oxide,[189] graphitic carbon nitride,[190,191] black phosphorus sheets,[58,192] and carbon nanofiber[193–195] can enhance the catalytic performance of amorphous TM borides. These substrates with large surface areas are deemed to disperse boride particles and thus enlarge the electroactive surface area. In addition, the interaction between borides and substrates can modify borides' electronic structures and upgrade the catalytic property.[193] For instance, the 2D/2D exfoliated black phosphorus (EBP) nanosheet/amorphous CoFeB nanosheets heterostructure (EBP/CoFeB) with wrinkled surface morphology prepared by a chemical reduction method (Figure 12A,B) manifests high OER activities ($\eta_{10} = 227$ mV, Figure 12C) with excellent stability in the basic electrolyte. In-depth investigations indicate that the electronic interactions and O affinity difference between CoFeB and EBP can balance the absorption behavior of reaction intermediate for improving the OER and MOR process (Figure 12D).[58] By tuning the absorption strength of oxygen-containing intermediates, BP-based heterostructures would significantly facilitate the catalytic process.

Some studies also have used electroactive materials to support amorphous TM borides, such as Ni hydroxide[196] and pyrite-type boron sulfide.[197] With a chemical surface etching process, the Ni hydroxide phase was formed together with the metallic NiB phase.[196] The obtained F-Ni_2B/Ni$(OH)_x$ catalyst with two phases coexisting on the surface can utilize the abundant adsorption sites in the Ni$(OH)_x$ phase as well as the excellent electrical

conductivity of the Ni_2B phase. Thus, the F-Ni_2B/$Ni(OH)_x$ composite outperforms the single Ni_2B and the noble metal-based RuO_2 catalyst for OER (Figure 12E,F). In the amorphous $FeCoNiB_x$ coated ternary pyrite-type boron sulfide ($FeCoNiB_x/Ni_{0.8}Fe_{0.1}Co_{0.1}S_2B_x$) catalyst, B atoms reconfigure the electronic structure of metals via downshifting the d-band center and regulating intermediates' binding energies.[197] Moreover, the metallic boride coating enhances the conductivity for OER, and thus, a high activity is attained (η_{50} = 392.4 mV).

7.3 | TM oxometallates

Amorphous TM oxometallates with rich oxygen components such as phosphates,[64] borates,[198] selenites,[199] and silicates[49] are emerging electrocatalysts for ESM. It is suggested that the oxyanions (e.g., PO_4^{3-} and BO_3^{3-}) of TM oxometallates with large negative charges can serve as proton carriers and facilitate the proton transfer process; also, they can stabilize the local pH environment during ESM.[200–202] The development of TM oxometallates-based catalysts mainly concentrates on nanostructure design, heteroatom doping, and heterostructure construction.

7.3.1 | Nanostructure design

To achieve an excellent ESM activity, endowing catalysts with architectural merits like high surface area and rational pore hierarchy is a sound option. In this context, porous 2D nanosheets,[203] 3D nanostructures,[204] and hierarchical nanostructures[63] are preferred choices. Starting from 2D Co phosphonate organic frameworks, Guo et al. developed amorphous Co phosphate porous nanosheets via calcination.[205] The porous structure provides the amorphous Co phosphate with a large free space, increased the distribution of electroactive centers, and facilitated hydroxide diffusion during the OER process. Similarly, in a microporous 2D NiCoFe phosphate nanosheet catalyst, the microporous confinement in a 2D orientation would decrease the resistance of mass transport, enlarge the ECSA, and enhance the diffusion of O_2 products.[206] The study by Dastafkan et al. suggests that the amorphous iron borate film shows high surface wettability that facilitates efficient O_2 dissipation and improved mass transfer during OER.[207] In addition, the 3D hierarchical structure of nickel borate contributes to high UOR performance.[208] Hence, the multiple effects of nanostructure on catalysts' properties (e.g., surface area, surface wettability, and reactant/product transportation) should be thoroughly checked in further catalyst design.

7.3.2 | Heteroatom doping

Doping is widely applied to regulate the electronic properties of materials, which can further tune the intrinsic catalytic performance. Both anionic and cationic dopings have been implemented to boost amorphous TM oxometallates' ESM performance. For example, Wang et al. developed an N-doped amorphous CoFe selenites catalyst through a hydrothermal treatment–calcination process.[46] The N-dopant can tailor the electronic structure of CoFe selenites and thus leads to a high OER performance (η_{10} = 242 mV, Tafel slope = 59.1 mV dec^{-1}). Compared with anionic doping, cationic doping is more prevalent, and the most frequently used dopants are Fe and Ni.[44,64,209,210] Generally, cationic doping can improve the electrical conductivity and modify catalysts' electronic structures, thereby upgrading the catalytic performance. In addition, Yang et al. suggested that the Ni dopants in Co phosphate can promote the in situ surface reconstruction evolving into electroactive metal oxyhydroxides under the OER conditions.[64]

7.3.3 | Heterostructure construction

Amorphous TM oxometallates-based hybrids have been well studied for ESM. In most cases, the amorphous TM oxometallates are coated onto the surface of electroactive materials or conductive carbons.[198,211,212] In an amorphous NiFe-borate layer covered NiFe LDH nanoarray (NiFe-LDH@NiFe-Bi) catalyst, the amorphous NiFe–Bi shell significantly promotes the evolution of electroactive NiOOH phases on NiFe-LDH surface.[213] Differently, in the crystalline Ni phosphate ($Ni(PO_3)_2$)@amorphous CoFe phosphate (CoFePi) catalyst developed by a hydrothermal process-dipping-phosphorization method (Figure 13A),[48] the sufficient electroactive sites, excellent electrical conductivity, and high structural stability arise from the amorphous–crystalline composite contribute to its good OER performance. Amorphous TM oxometallates/carbon hybrids can be synthesized in a more facile way; as shown in Figure 13B, the Co borate (Co-Bi)/graphene composite was obtained with a chemical reduction process.[214] In the Co-Bi/graphene heterostructure, the graphene supports can not only guide the formation of 2D ultrathin borate nanosheet structure but also expedite electron transfer to promote OER kinetics. Moreover, the synergistic coupled effects between graphene and Co-Bi support charge transport, thereby contributing to superior OER performance in both alkaline and neutral solutions. The structure reconstruction of amorphous TM oxometallates/carbon hybrids has been examined on the amorphous Fe-doped Ni phosphate–carbon nanohybrid

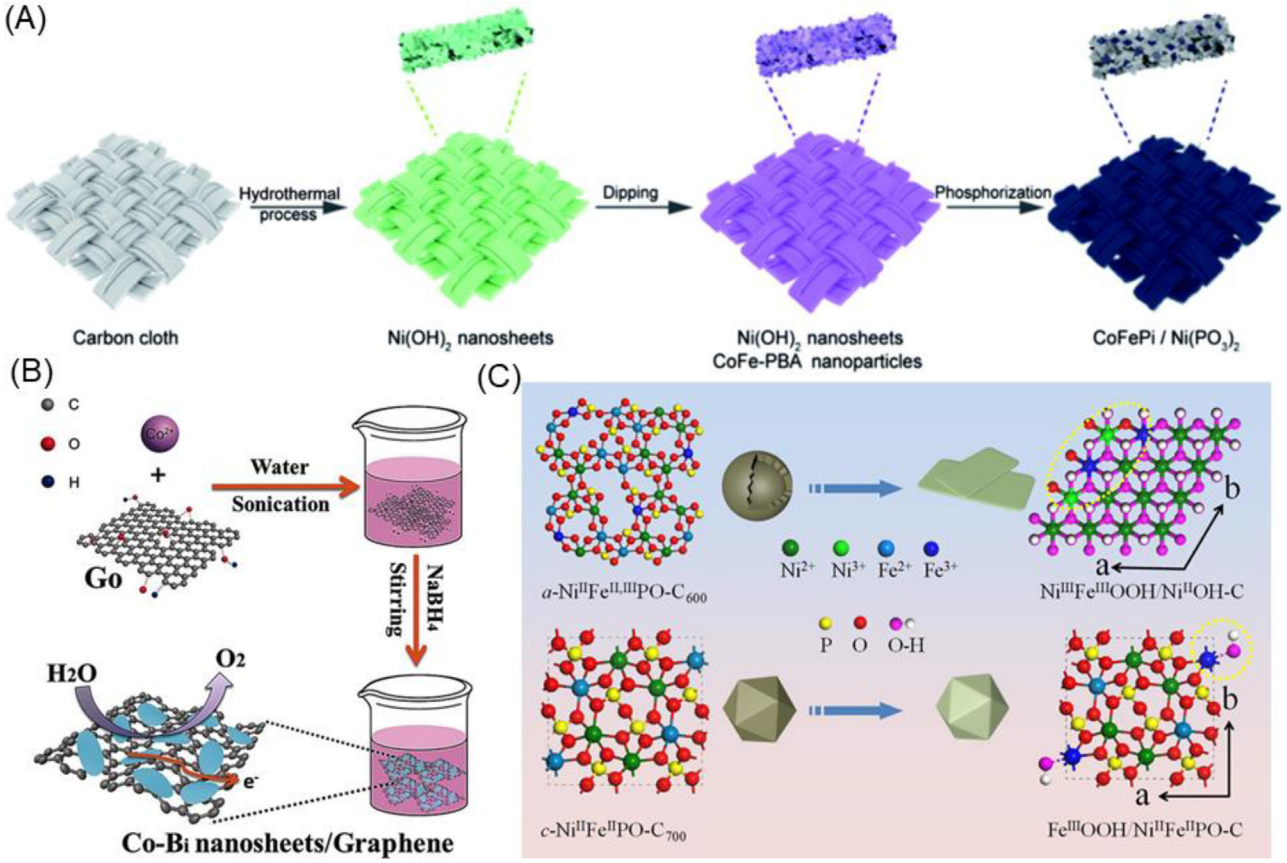

FIGURE 13 (A) Scheme of the preparation of the CoFePi/$Ni(PO_3)_2$ composite with a three-stage synthetic approach. (B) Illustration of synthesis of Co borate nanosheets grown on graphene sheets. (C) Structure reconstruction of amorphous and crystalline iron-doped nickel phosphate–carbon catalysts. *Source*: (A) Reproduced with permission: Copyright 2018, Royal Society of Chemistry.[48] (B) Reproduced with permission: Copyright 2016, Wiley-VCH.[214] (C) Reproduced with permission: Copyright 2021, American Chemical Society.[215]

(a-NiFePO-C).[215] Compared with its crystalline counterpart, the higher OER activities of a-NiFePO-C are due to its more complete self-reconstruction induced highly electroactive Fe(III)-NiOOH-carbon structures (Figure 13C), and low charge-transfer resistance.

8 | CONCLUSIONS AND PERSPECTIVES

Designing efficient amorphous low-cost ESM catalysts is an urgent task in advancing hydrogen energy. This review provides a critical analysis of recent achievements in the design of amorphous TM-based catalysts for ESM. The main features of amorphous catalysts include large SSA, flexible electronic structure, and deep structure reconstruction. Powerful catalyst design strategies such as nanostructure design, component regulation, heteroatom doping, and heterostructure construction have been successfully implemented to design efficient TM alloys, (hydr)oxides, chalcogenides, phosphides, nitrides, borides, and oxometallates for ESM (Scheme 2). These strategies can efficiently improve the catalytic performance of amorphous materials by providing more electroactive sites, ensuring fast mass/charge transfer, enlarging ECSA, regulating catalysts' electronic properties, and improving the structure stability.

Despite current achievements, some critical issues deserve further study:

1. Developing new techniques to realize the large-scale production of low-cost amorphous electrocatalysts is highly urgent. Reducing amorphous TM-based electrocatalysts' fabrication costs is an urgent mission, which would largely improve their cost-effectiveness. Given the environmental impact of catalyst preparation, it is favorable to employ methods with low energy consumption and/or carbon emissions such as chemical precipitation, electrodeposition, flash Joule heating, ball milling, and plasma synthesis. In addition, it is necessary to design protocols for large-scale catalyst preparation to meet the demand of industrial applications.
2. Innovating novel catalyst design strategies to enhance catalytic performance is necessary. Compared with one

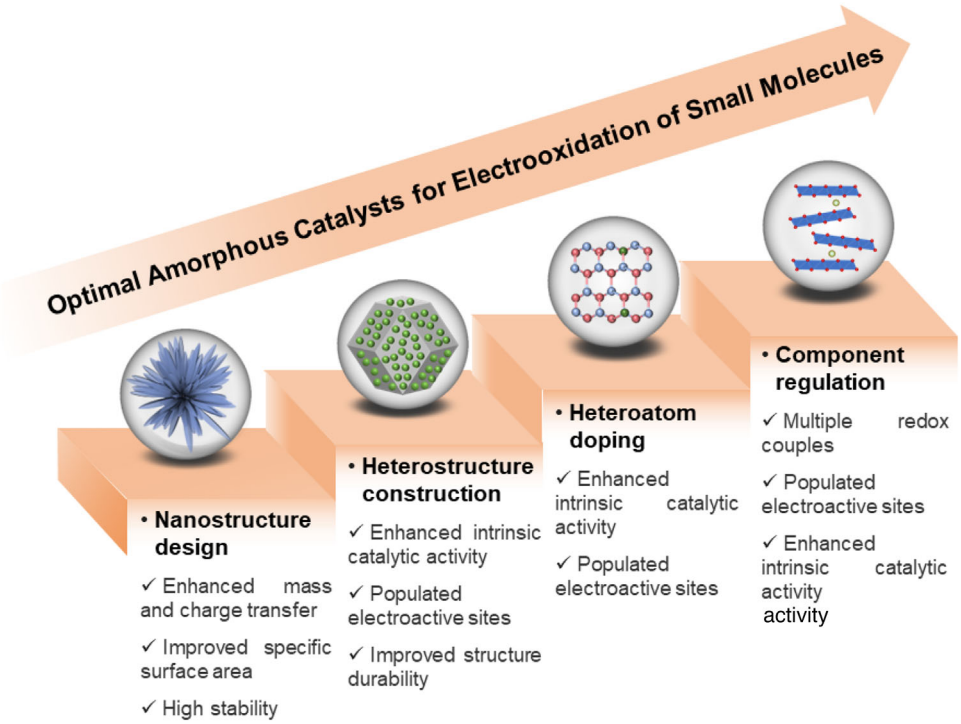

SCHEME 2 A summary of key strategies for amorphous electrocatalyst design.

individual strategy (e.g., doping, nanostructure control, heterostructure construction, or component optimization), the co-implementation of multiple strategies would combine the advantages of individuals and lead to optimal catalysts. Considering the rapid development of single-atom catalysts, combining single/dual-atom catalysts with amorphous TM nanomaterials might lead to highly efficient catalysts for ESM. Moreover, by combining the catalytic properties of different metals, the development of amorphous high entropy catalysts would generate novel catalyst systems.

3. It is suggested to utilize different advanced techniques (e.g., X-ray absorption spectroscopy, high-resolution transmission electron microscopy, and DFT calculations) to figure out the fine structure of amorphous catalysts, which could assist the interpretation of the structure-performance relationship and guide future catalyst design. Of note, it is still challenging to determine the exact structure of amorphous catalysts due to the feature of long-range disorder, which significantly hinders the computations of amorphous catalysts. In this context, it is necessary to figure out the structure of amorphous materials with advanced X-ray techniques (e.g., X-ray absorption spectroscopy), atomic electron tomography, fluctuation electron microscopy, and so on before performing DFT calculations and molecular dynamics simulations. Another issue is that most TM-based catalysts undergo in situ structure self-reconstruction during electrooxidation processes, and thus, it is important to track catalysts' structure self-transformation and understand the dynamic evolution of electroactive sites.
4. Implementing amorphous catalysts in industrial applications is necessary for their further applications. Currently, most electrochemical tests are performed on a laboratory scale, which is far from industrial conditions. Accordingly, measuring catalysts' activities at high current densities and long testing periods would help to take catalysts' application one step further. This requires the development of high-performance catalysts and large-scale electrochemical reactors. Aside from water electrolysis that only produces high-purity gaseous products, the electrolysis of alcohols and complex biomass will generate value-added liquid products that require separation and purification facilities.
5. Aside from electrochemical oxidation of small molecules to produce value-added chemicals/fuels, it is significant to apply amorphous catalysts in other fields to address pressing environmental and energy challenges, such as inorganic/organic pollutant oxidation/reduction, oxygen reduction, carbon dioxide/carbon monoxide reduction, nitrogen/nitrate reduction, hydrogen oxidation, and biowaste conversion. With high redox properties and low cost, amorphous TM-based catalysts would help to improve the catalytic reaction efficiency and save energy input for different applications.

ACKNOWLEDGMENTS

This work is supported by the Australian Research Council (ARC) Discovery Project (DP220101139). Dr. Wei Wei acknowledges the support of the Australian Research Council (ARC) through Project DE220100530.

CONFLICT OF INTEREST STATEMENT

The authors declare no conflicts of interest.

ORCID

Zhijie Chen https://orcid.org/0000-0003-0627-0856
Ning Han https://orcid.org/0000-0003-0920-9049
Bing-Jie Ni https://orcid.org/0000-0002-1129-7837

REFERENCES

1. Wang T, Cao X, Jiao L. Progress in hydrogen production coupled with electrochemical oxidation of small molecules. *Angew Chem Int Ed*. 2022;61:e202213328.
2. Chen Z, Yun S, Wu L, et al. Waste-derived catalysts for water electrolysis: circular economy-driven sustainable green hydrogen energy. *Nano-Micro Lett*. 2023;15:4.
3. Zhu B, Liang Z, Zou R. Designing advanced catalysts for energy conversion based on urea oxidation reaction. *Small*. 2020;16(7):e1906133.
4. Gnana Kumar G, Farithkhan A, Manthiram A. Direct urea fuel cells: recent progress and critical challenges of urea oxidation electrocatalysis. *Adv Energy Sustainability Res*. 2020;1(1):2000015.
5. Chen Z, Wei W, Song L, Ni B-J. Hybrid water electrolysis: a new sustainable avenue for energy-saving hydrogen production. *Sustainable Horiz*. 2022;1:100002.
6. Jiang X, Li W, Liu Y, et al. Electrocatalytic oxidation of 5-hydroxymethylfurfural for sustainable 2,5-furandicarboxylic acid production-From mechanism to catalysts design. *SusMat*. 2023;3(1):21-43.
7. Jenewein KJ, Knöppel J, Hofer A, et al. Dissolution of WO_3 modified with IrO_x overlayers during photoelectrochemical water splitting. *SusMat*. 2023;3(1):128-136.
8. Chen Z, Zheng R, Deng S, et al. Modular design of an efficient heterostructured FeS_2/TiO_2 oxygen evolution electrocatalyst via sulfidation of natural ilmenites. *J Mater Chem A*. 2021;9(44):25032-25041.
9. Mirshokraee SA, Muhyuddin M, Lorenzi R, et al. Litchi-derived platinum group metal-free electrocatalysts for oxygen reduction reaction and hydrogen evolution reaction in alkaline media. *SusMat*. 2023;3(2):248-262.
10. Chen Z, Wei W, Ni B-J, Chen H. Plastic wastes derived carbon materials for green energy and sustainable environmental applications. *Environ Funct Mater*. 2022;1(1):34-48.
11. Wang Q, Han N, Shen Z, et al. MXene-based electrochemical (bio) sensors for sustainable applications: roadmap for future advanced materials. *Nano Mater Sci*. 2022;5(1):39-52.
12. Guo T, Li L, Wang Z. Recent development and future perspectives of amorphous transition metal-based electrocatalysts for oxygen evolution reaction. *Adv Energy Mater*. 2022;12(24):2200827.
13. Zhang J, Yu P, Zeng G, Bao F, Yuan Y, Huang H. Boosting HMF oxidation performance via decorating ultrathin nickel hydroxide nanosheets with amorphous copper hydroxide islands. *J Mater Chem A*. 2021;9(15):9685-9691.
14. Crousier J, Crousier J, Bellucci F. Electrochemical and electrocatalytic behaviour of iron-base amorphous alloys in 1 M KOH at 25°C. *Electrochim Acta*. 1993;38(6):821-825.
15. Shobba T, Mayanna S, Sequeira C. Preparation and characterization of Co–W alloys as anode materials for methanol fuel cells. *J Power Sources*. 2002;108(1):261-264.
16. Lu X, Zhu J. Amorphous ceramic material as sulfur-tolerant anode for SOFC. *J Electrochem Soc*. 2008;155(10):B1053.
17. Zheng Y-X, Yao S-B, Zhou S-M. Electrooxidation of ethanol at Ni-B amorphous alloy electrode and measurements of kinetic parameters. *Acta Phys Chim Sin*. 2008;24(9):1643-1649.
18. Chen C, Zhu S, Yang X, Pi L, Cui Z. Electro-oxidation of ethylene glycol on nanoporous Ti–Cu amorphous alloy. *Electrochim Acta*. 2011;56(27):10253-10258.
19. Wang H, Ma Y, Wang R, Key J, Linkov V, Ji S. Liquid–liquid interface-mediated room-temperature synthesis of amorphous NiCo pompoms from ultrathin nanosheets with high catalytic activity for hydrazine oxidation. *Chem Commun*. 2015;51(17):3570-3573.
20. Xie J, Qu H, Lei F, et al. Partially amorphous nickel–iron layered double hydroxide nanosheet arrays for robust bifunctional electrocatalysis. *J Mater Chem A*. 2018;6(33):16121-16129.
21. Song X, Liu X, Wang H, Guo Y, Wang Y. Improved performance of nickel boride by phosphorus doping as an efficient electrocatalyst for the oxidation of 5-hydroxymethylfurfural to 2,5-furandicarboxylic acid. *Ind Eng Chem Res*. 2020;59(39):17348-17356.
22. Vo T-G, Ho P-Y, Chiang C-Y. Operando mechanistic studies of selective oxidation of glycerol to dihydroxyacetone over amorphous cobalt oxide. *Appl Catal B: Environ*. 2022;300:120723.
23. Yan S, Zhong M, Wang C, Lu X. Amorphous aerogel of trimetallic FeCoNi alloy for highly efficient oxygen evolution. *Chem Eng J*. 2022;430:132955.
24. Wang Y, Zhou Y, Han M, et al. Environmentally-friendly exfoliate and active site self-assembly: thin 2D/2D heterostructure amorphous nickel–iron alloy on 2D materials for efficient oxygen evolution reaction. *Small*. 2019;15(16):1805435.
25. Le T-H-H, Vo T-G, Chiang C-Y. Highly efficient amorphous binary cobalt-cerium metal oxides for selective oxidation of 5-hydroxymethylfurfural to 2,5-diformylfuran. *J Catal*. 2021;404:560-569.
26. Zhang W, Chen G, Du Y, et al. Large-scale synthesis of Fe-doped amorphous cobalt oxide electrocatalysts at room temperature for the oxygen evolution reaction. *ACS Appl Energy Mater*. 2022;5(3):3129-3136.
27. Gao L, Xie J, Liu S, et al. Crystalline cobalt/amorphous $LaCoO_x$ hybrid nanoparticles embedded in porous nitrogen-doped carbon as efficient electrocatalysts for hydrazine-assisted hydrogen production. *ACS Appl Mater Interfaces*. 2020;12(22):24701-24709.
28. Cao X, Wang T, Qin H, Lin G, Zhao L, Jiao L. Crystalline–amorphous interfaces of NiO-CrO_x electrocatalysts for boosting the urea oxidation reaction. *Nano Res*. 2023;16(3):3665-3671.
29. Shang X, Yan K-L, Lu S-S, et al. Controlling electrodeposited ultrathin amorphous Fe hydroxides film on V-doped nickel

sulfide nanowires as efficient electrocatalyst for water oxidation. *J Power Sources*. 2017;363:44-53.

30. Jiang Y, Gao S, Xu G, Song X. Porous and amorphous cobalt hydroxysulfide core–shell nanoneedles on Ti-mesh as a bifunctional electrocatalyst for energy-efficient hydrogen production via urea electrolysis. *J Mater Chem A*. 2021;9(9):5664-5674.
31. Liu W, Liu H, Dang L, et al. Amorphous cobalt–iron hydroxide nanosheet electrocatalyst for efficient electrochemical and photo-electrochemical oxygen evolution. *Adv Funct Mater*. 2017;27(14):1603904.
32. Huang X, Guo Y, Zou Y, Jiang J. Electrochemical oxidation of glycerol to hydroxypyruvic acid on cobalt (oxy)hydroxide by high-valent cobalt redox centers. *Appl Catal B: Environ*. 2022;309:121247.
33. Yuan G, Hu Y, Wang Q, et al. Tuning the morphological and electronic structure of amorphous nickel-based electrocatalysts by anion regulation for water oxidation in neutral media. *Inorg Chem Front*. 2019;6(11):3093-3096.
34. Qin M, Li Y, Zhang H, et al. Crystalline/amorphous heterostructure offering highly efficient overall water splitting and urea electrolysis. *J Alloys Compd*. 2022;921:166071.
35. Sun Y, Wang S, Ning J, Zhang Z, Zhong Y, Hu Y. A one-pot "shielding-to-etching" strategy to synthesize amorphous MoS_2 modified $CoS/Co_{0.85}Se$ heterostructured nanotube arrays for boosted energy-saving H_2 generation. *Nanoscale*. 2020;12(2):991-1001.
36. Yi X, He X, Yin F, Chen B, Li G, Yin H. Amorphous Ni–Fe–Se hollow nanospheres electrodeposited on nickel foam as a highly active and bifunctional catalyst for alkaline water splitting. *Dalton Trans*. 2020;49(2):6764-6775.
37. Park KR, Tran DT, Nguyen TT, Kim NH, Lee JH. Copper-Incorporated heterostructures of amorphous $NiSe_x$/crystalline $NiSe_2$ as an efficient electrocatalyst for overall water splitting. *Chem Eng J*. 2021;422:130048.
38. Zhang J, Cao X, Guo M, et al. Unique Ni crystalline core/Ni phosphide amorphous shell heterostructured electrocatalyst for hydrazine oxidation reaction of fuel cells. *ACS Appl Mater Interfaces*. 2019;11(21):19048-19055.
39. Sun Q, Zhou M, Shen Y, et al. Hierarchical nanoporous Ni(Cu) alloy anchored on amorphous NiFeP as efficient bifunctional electrocatalysts for hydrogen evolution and hydrazine oxidation. *J Catal*. 2019;373:180-189.
40. Hu F, Zhu S, Chen S, et al. Amorphous metallic NiFeP: a conductive bulk material achieving high activity for oxygen evolution reaction in both alkaline and acidic media. *Adv Mater*. 2017;29(32):1606570.
41. Tong Y, Chen L, Dyson PJ, Fei Z. Boosting hydrogen production via urea electrolysis on an amorphous nickel phosphide/graphene hybrid structure. *J Mater Sci*. 2021;56(31):17709-17720.
42. Chen Z, Zheng R, Graś M, et al. Tuning electronic property and surface reconstruction of amorphous iron borides via W-P co-doping for highly efficient oxygen evolution. *Appl Catal B: Environ*. 2021;288:120037.
43. Lu S, Cao D, Xu X, Wang H, Xiang Y. Study of carbon black supported amorphous Ni–B nano-catalyst for hydrazine electrooxidation in alkaline media. *RSC Adv*. 2014;4(51):26940-26945.
44. Han J, Wei Q, Zhang J, et al. The triple structure design of 2D amorphous Fe-doped indium phosphate nanosheets as a highly efficient electrocatalyst for water oxidation. *J Mater Chem A*. 2020;8(35):18232-18243.
45. Khalaf MM, Abd El-Lateef HM, Dao V-D, Mohamed IM. Electrocatalysis of methanol oxidation in alkaline electrolytes over novel amorphous Fe/Ni biphosphate material prepared by different techniques. *Nanomaterials*. 2022;12(19):3429.
46. Wang B, Zhou L-L, Huang Z-Q, Pan D-S, Guo Z-H, Song J-L. In situ construction of N-doped amorphous CoFe selenites toward efficient electrocatalytic water oxidation. *J Power Sources*. 2021;483:229196.
47. Chen L, Ren X, Teng W, Shi P. Amorphous nickel-cobalt-borate nanosheet arrays for efficient and durable water oxidation electrocatalysis under near-neutral conditions. *Chem Eur J*. 2017;23(41):9741-9745.
48. Liu D-C, Cao L-M, Luo Z-M, Zhong D-C, Tan J-B, Lu T-B. An in situ generated amorphous CoFePi and crystalline $Ni(PO_3)_2$ heterojunction as an efficient electrocatalyst for oxygen evolution. *J Mater Chem A*. 2018;6(48):24920-24927.
49. Kim B, Kim JS, Kim H, Park I, Seong WM, Kang K. Amorphous multinary phyllosilicate catalysts for electrochemical water oxidation. *J Mater Chem A*. 2019;7(31):18380-18387.
50. Zhang D, Soo JZ, Tan HH, Jagadish C, Catchpole K, Karuturi SK. Earth-abundant amorphous electrocatalysts for electrochemical hydrogen production: a review. *Adv Energy Sustainability Res*. 2021;2(3):2000071.
51. Anantharaj S, Noda S. Amorphous catalysts and electrochemical water splitting: an untold story of harmony. *Small*. 2019;16(2):e1905779.
52. Zhou H, Zheng M, Tang H, Xu B, Tang Y, Pang H. Amorphous intermediate derivative from ZIF-67 and its outstanding electrocatalytic activity. *Small*. 2020;16(2):1904252.
53. Li X, Zhang H, Hu Q, et al. Amorphous NiFe oxide-based nanoreactors for efficient electrocatalytic water oxidation. *Angew Chem Int Ed*. 2023;62:e202300478.
54. Duan Y, Yu Z-Y, Hu S-J, et al. Scaled-up synthesis of amorphous NiFeMo oxides and their rapid surface reconstruction for superior oxygen evolution catalysis. *Angew Chem Int Ed*. 2019;58:15772-15777.
55. Wei Q, Tan X, Zhang J, Yang L, Cao L, Dong B. Fe doped amorphous single layered vanadyl phosphate nanosheets as highly efficient electrocatalyst for water oxidation. *J Colloid Interface Sci*. 2021;586:505-513.
56. Cai W, Chen R, Yang H, et al. Amorphous versus crystalline in water oxidation catalysis: a case study of NiFe alloy. *Nano Lett*. 2020;20(6):4278-4285.
57. Chen Z, Zou W, Zheng R, et al. Synergistic recycling and conversion of spent Li-ion battery leachate into highly efficient oxygen evolution catalysts. *Green Chem*. 2021;23(17):6538-6547.
58. Chen H, Chen J, Ning P, et al. 2D heterostructure of amorphous CoFeB coating black phosphorus nanosheets with optimal oxygen intermediate absorption for improved electrocatalytic water oxidation. *ACS Nano*. 2021;15(7):12418-12428.
59. Shi Z, Yu Z, Guo J, et al. Lattice distortion of crystalline-amorphous nickel molybdenum sulfide nanosheets for high-efficiency overall water splitting: libraries of lone pairs of electrons and in situ surface reconstitution. *Nanoscale*. 2022;14(4):1370-1379.

60. Bak J, Yun TG, An J-S, Bae HB, Chung S-Y. Comparison of Fe-enhanced oxygen evolution electrocatalysis in amorphous and crystalline nickel oxides to evaluate the structural contribution. *Energy Environ Sci*. 2022;15(2):610-620.
61. Wang Q, Li Y, Zhang C. Amorphous nickel oxide as efficient electrocatalyst for urea oxidation reaction. *J Electrochem Soc*. 2021;168(7):076502.
62. Xu S, Lv C, He T, Huang Z, Zhang C. Amorphous film of cerium doped cobalt oxide as a highly efficient electrocatalyst for oxygen evolution reaction. *J Mater Chem A*. 2019;7(13):7526-7532.
63. Liu Y, Zhang J, Wang W, Cao L, Dong B. Two-phase colloidal synthesis of amorphous iron-doped manganese phosphate hollow nanospheres for efficient water oxidation. *Adv Sustainable Syst*. 2020;4(11):2000128.
64. Yang L, Ren H, Liang Q, Dinh KN, Dangol R, Yan Q. Ultrathin amorphous nickel doped cobalt phosphates with highly ordered mesoporous structures as efficient electrocatalyst for oxygen evolution reaction. *Small*. 2020;16(7):1906766.
65. Hu J, Al-Salihy A, Wang J, et al. Improved interface charge transfer and redistribution in CuO-CoOOH p-n heterojunction nanoarray electrocatalyst for enhanced oxygen evolution reaction. *Adv Sci*. 2021;8(22):e2103314.
66. Chen Z, Zheng R, Zou H, et al. Amorphous iron-doped nickel boride with facilitated structural reconstruction and dual active sites for efficient urea electrooxidation. *Chem Eng J*. 2023;465:142684.
67. Zheng K, Ren J, Li X, Li G, Jiao L, Xu C. Engineering crystalline CoMP-decorated (M = Mn, Fe, Ni, Cu, Zn) amorphous CoM LDH for high-rate alkaline water splitting. *Chem Eng J*. 2022;441:136031.
68. Chen Z, Zheng R, Wei W, Wei W, Ni B-J, Chen H. Unlocking the electrocatalytic activity of natural chalcopyrite using mechanochemistry. *J Energy Chem*. 2022;68:275-283.
69. Kumar A, Muhommad J, Purkayastha SK, Guha AK, Das MR, Deka S. Robust and promising electrocatalytic oxygen evolution reaction by activated Cu–Co–B amorphous nanosheets. *ACS Sustainable Chem Eng*. 2023;11(6):2541-2553.
70. Yang D, Su Z, Chen Y, et al. Self-reconstruction of a MOF-derived chromium-doped nickel disulfide in electrocatalytic water oxidation. *Chem Eng J*. 2022;430:133046.
71. Baksi A, Nandam SH, Wang D, et al. $Ni_{60}Nb_{40}$ nanoglass for tunable magnetism and methanol oxidation. *ACS Appl Nano Mater*. 2020;3(7):7252-7259.
72. Chen Z, Duan X, Wei W, Wang S, Zhang Z, Ni B-J. Boride-based electrocatalysts: emerging candidates for water splitting. *Nano Res*. 2020;13(2):293-314.
73. Lian J, Wu Y, Sun J. High current density electrodeposition of NiFe/nickel foam as a bifunctional electrocatalyst for overall water splitting in alkaline electrolyte. *J Mater Sci*. 2020;55(31):15140-15151.
74. Niu C, Zhang Y, Dong J, Yuan R, Kou W, Xu L. 3D ordered macro-/mesoporous Ni_xCo_{100-x} alloys as high-performance bifunctional electrocatalysts for overall water splitting. *Chin Chem Lett*. 2021;32(8):2484-2488.
75. Xu L, Zhang F-T, Chen J-H, Fu X-Z, Sun R, Wong C-P. Amorphous NiFe nanotube arrays bifunctional electrocatalysts for efficient electrochemical overall water splitting. *ACS Appl Energy Mater*. 2018;1(3):1210-1217.
76. Abdolmaleki M, Bodaghi A, Hosseini J, Jamehbozorgi S. Preparation of nanostructured Co–Mo alloy electrodes and investigation of their electrocatalytic activity for hydrazine oxidation in alkaline medium. *J Chin Chem Soc*. 2018;65(8):970-976.
77. Tang P-P, Lin X, Yin H, et al. Hierarchically nanostructured nickel–cobalt alloy supported on nickel foam as a highly efficient electrocatalyst for hydrazine oxidation. *ACS Sustainable Chem Eng*. 2020;8(44):16583-16590.
78. Zhu W, Zhu G, Yao C, et al. Porous amorphous FeCo alloys as pre-catalysts for promoting the oxygen evolution reaction. *J Alloys Compd*. 2020;828:154465.
79. Chen Z, Duan X, Wei W, Wang S, Ni B-J. Electrocatalysts for acidic oxygen evolution reaction: achievements and perspectives. *Nano Energy*. 2020;78:105392.
80. Liu J, Ji Y, Nai J, et al. Ultrathin amorphous cobalt–vanadium hydr(oxy)oxide catalysts for the oxygen evolution reaction. *Energy Environ Sci*. 2018;11(7):1736-1741.
81. Chen Z, Wei W, Chen H, Ni B-J. Eco-designed electrocatalysts for water splitting: a path toward carbon neutrality. *Int J Hydrogen Energy*. 2023;48(16):6288-6307.
82. Pan L, Wang Q, Li Y, Zhang C. Amorphous cobalt-cerium binary metal oxides as high performance electrocatalyst for oxygen evolution reaction. *J Catal*. 2020;384:14-21.
83. Sial MAZG, Baskaran S, Jalil A, et al. NiCoFe oxide amorphous nanohetrostructres for oxygen evolution reaction. *Int J Hydrogen Energy*. 2019;44(41):22991-23001.
84. Han N, Feng S, Liang Y, et al. Achieving efficient electrocatalytic oxygen evolution in acidic media on yttrium ruthenate pyrochlore through cobalt incorporation. *Adv Funct Mater*. 2023:2208399.
85. Indra A, Menezes PW, Sahraie NR, et al. Unification of catalytic water oxidation and oxygen reduction reactions: amorphous beat crystalline cobalt iron oxides. *J Am Chem Soc*. 2014;136(50):17530-17536.
86. Wang L, Geng J, Wang W, Yuan C, Kuai L, Geng B. Facile synthesis of Fe/Ni bimetallic oxide solid-solution nanoparticles with superior electrocatalytic activity for oxygen evolution reaction. *Nano Res*. 2015;8(12):3815-3822.
87. Kuai L, Geng J, Chen C, et al. A reliable aerosol-spray-assisted approach to produce and optimize amorphous metal oxide catalysts for electrochemical water splitting. *Angew Chem Int Ed*. 2014;126(29):7677-7681.
88. Daemi S, Moalem-Banhangi M, Ghasemi S, Ashkarran AA. An efficient platform for the electrooxidation of formaldehyde based on amorphous $NiWO_4$ nanoparticles modified electrode for fuel cells. *J Electroanal Chem*. 2019;848:113270.
89. Yang Y, Fei H, Ruan G, Xiang C, Tour JM. Efficient electrocatalytic oxygen evolution on amorphous nickel–cobalt binary oxide nanoporous layers. *ACS Nano*. 2014;8(9):9518-9523.
90. Bai L, Wen X, Guan J. Amorphous FeCoNi oxide for oxygen evolution reaction. *Mater Today Energy*. 2019;12:311-317.
91. Chen C-W, Chiang C-Y. Molybdenum-containing amorphous metal oxide catalysts for oxygen evolution reaction. *Int J Hydrogen Energy*. 2017;42(50):29773-29780.
92. Zhang C, Berlinguette CP, Trudel S. Water oxidation catalysis: an amorphous quaternary Ba-Sr-Co-Fe oxide as a promising electrocatalyst for the oxygen-evolution reaction. *Chem Commun*. 2016;52(7):1513-1516.
93. Guo C, Sun X, Kuang X, et al. Amorphous Co-doped MoO_x nanospheres with a core–shell structure toward an effective oxygen evolution reaction. *J Mater Chem A*. 2019;7(3):1005-1012.

94. Xiong S, Wang L, Chai H, Xu Y, Jiao Y, Chen J. Molybdenum doped induced amorphous phase in cobalt acid nickel for supercapacitor and oxygen evolution reaction. *J Colloid Interface Sci*. 2022;606:1695-1706.
95. Wang X, Xing C, Liang Z, et al. Activating the lattice oxygen oxidation mechanism in amorphous molybdenum cobalt oxide nanosheets for water oxidation. *J Mater Chem A*. 2022;10(7):3659-3666.
96. Guo Z, Pang Y, Xie H, He G, Parkin IP, Chai G-L. Phosphorus-doped $CuCo_2O_4$ oxide with partial amorphous phase as a robust electrocatalyst for the oxygen evolution reaction. *ChemElectroChem*. 2021;8(1):135-141.
97. Kim K, Kang T, Kim M, Kim J. Exploring the intrinsic active sites and multi oxygen evolution reaction step via unique hollow structures of nitrogen and sulfur co-doped amorphous cobalt and nickel oxides. *Chem Eng J*. 2021;426:130820.
98. Dong Z, Lin F, Yao Y, Jiao L. Crystalline $Ni(OH)_2$/amorphous $NiMoO_x$ mixed-catalyst with Pt-like performance for hydrogen production. *Advanced Energy Materials*. 2019;9(46):1902703.
99. Liu X, Duan X, Bao T, et al. High-performance photocatalytic decomposition of PFOA by BiO_X/TiO_2 heterojunctions: self-induced inner electric fields and band alignment. *J Hazard Mater*. 2022;430:128195.
100. Zeng L, Thiruppathi AR, van der Zalm J, Shi T, Chen A. Tailoring trimetallic CoNiFe oxide nanostructured catalysts for the efficient electrochemical conversion of methane to methanol. *J Mater Chem A*. 2022;10(28):15012-15025.
101. Yan X, Liu Y, Lan J, et al. Crystalline–amorphous Co@CoO core–shell heterostructures for efficient electro-oxidation of hydrazine. *Mater Chem Front*. 2018;2(1):96-101.
102. Qiao L, Zhu A, Liu D, et al. Crystalline phosphides/amorphous oxides composite for energy-saving hydrogen production assisted by efficient urea oxidation reaction. *Chem Eng J*. 2023;454:140380.
103. Xu H, Zhang W-D, Yao Y, et al. Amorphous chromium oxide confined Ni/NiO nanoparticles-assembled nanosheets for highly efficient and stable overall urea splitting. *J Colloid Interface Sci*. 2023;629:501-510.
104. Yin Z, He R, Zhang Y, et al. Electrochemical deposited amorphous FeNi hydroxide electrode for oxygen evolution reaction. *J Energy Chem*. 2022;69:585-592.
105. Thangavel P, Kim G, Kim KS. Electrochemical integration of amorphous NiFe (oxy)hydroxides on surface-activated carbon fibers for high-efficiency oxygen evolution in alkaline anion exchange membrane water electrolysis. *J Mater Chem A*. 2021;9(24):14043-14051.
106. Chen Z, Wei W, Zou W, et al. Integrating electrodeposition with electrolysis for closing loop resource utilization of battery industrial wastewater. *Green Chem*. 2022;44:3208-3217.
107. Lee E, Park A-H, Park H-U, Kwon Y-U. Facile sonochemical synthesis of amorphous NiFe-(oxy) hydroxide nanoparticles as superior electrocatalysts for oxygen evolution reaction. *Ultrason Sonochem*. 2018;40:552-557.
108. Xu Y, Ren K, Xu R. In situ formation of amorphous Fe-based bimetallic hydroxides from metal-organic frameworks as efficient oxygen evolution catalysts. *Chin J Catal*. 2021;42(8):1370-1378.
109. Babar P, Lokhande A, Karade V, et al. Trifunctional layered electrodeposited nickel iron hydroxide electrocatalyst with enhanced performance towards the oxidation of water, urea and hydrazine. *J Colloid Interface Sci*. 2019;557:10-17.
110. Zhang J, Gong W, Yin H, et al. Situ growth of ultrathin $Ni(OH)_2$ nanosheets as catalyst for electrocatalytic oxidation reactions. *ChemSusChem*. 2021;14(14):2935-2942.
111. Babar P, Patil K, Lee DM, et al. Cost-effective and efficient water and urea oxidation catalysis using nickel-iron oxyhydroxide nanosheets synthesized by an ultrafast method. *J Colloid Interface Sci*. 2021;584:760-769.
112. Tian T, Zheng M, Lin J, Meng X, Ding Y. Amorphous Ni–Fe double hydroxide hollow nanocubes enriched with oxygen vacancies as efficient electrocatalytic water oxidation catalysts. *Chem Commun*. 2019;55(8):1044-1047.
113. Ding J, Fan T, Shen K, Li Y. Electrochemical synthesis of amorphous metal hydroxide microarrays with rich defects from MOFs for efficient electrocatalytic water oxidation. *Appl Catal B: Environ*. 2021;292:120174.
114. Cai Z, Li L, Zhang Y, et al. Amorphous nanocages of Cu-Ni-Fe hydr(oxy)oxide prepared by photocorrosion for highly efficient oxygen evolution. *Angew Chem Int Ed*. 2019;58(13):4189-4194.
115. Balram A, Zhang H, Santhanagopalan S. Enhanced oxygen evolution reaction electrocatalysis via electrodeposited amorphous α-phase nickel-cobalt hydroxide nanodendrite forests. *ACS Appl Mater Interfaces*. 2017;9(34):28355-28365.
116. Liang H, Gandi AN, Xia C, et al. Amorphous NiFe-OH/NiFeP electrocatalyst fabricated at low temperature for water oxidation applications. *ACS Energy Lett*. 2017;2(5):1035-1042.
117. Zou X, Liu Y, Li G-D, et al. Ultrafast formation of amorphous bimetallic hydroxide films on 3D conductive sulfide nanoarrays for large-current-density oxygen evolution electrocatalysis. *Adv Mater*. 2017;29(22):1700404.
118. Lv Q, Yao B, Zhang W, et al. Controlled direct electrodeposition of crystalline NiFe/amorphous NiFe-(oxy)hydroxide on NiMo alloy as a highly efficient bifunctional electrocatalyst for overall water splitting. *Chem Eng J*. 2022;446:137420.
119. Liu C, Han Y, Yao L, et al. Engineering bimetallic NiFe-based hydroxides/selenides heterostructure nanosheet arrays for highly-efficient oxygen evolution reaction. *Small*. 2021;17(7):2007334.
120. Li Q, Chen Q, Lei S, et al. Crystalline Ni-Fe phosphide/amorphous P doped Fe-(oxy)hydroxide heterostructure as a multifunctional electrocatalyst for solar cell-driven hydrogen production. *J Colloid Interface Sci*. 2023;631:56-65.
121. Chen Z, Duan X, Wei W, Wang S, Ni B-J. Iridium-based nanomaterials for electrochemical water splitting. *Nano Energy*. 2020;78:105270.
122. Selvam NCS, Du L, Xia BY, Yoo PJ, You B. Reconstructed water oxidation electrocatalysts: the impact of surface dynamics on intrinsic activities. *Adv Funct Mater*. 2021;31(12):2008190.
123. Zhao G, Yao Y, Lu W, et al. Direct observation of oxygen evolution and surface restructuring on Mn_2O_3 nanocatalysts using in situ and ex situ transmission electron microscopy. *Nano Lett*. 2021;21(16):7012-7020.
124. Chen Z, Zheng R, Li S, et al. Dual-anion etching induced in situ interfacial engineering for high-efficiency oxygen evolution. *Chem Eng J*. 2022;431:134304.
125. Yang Y, Zhu B, Guo P-F, et al. Core-shell trimetallic NiFeV disulfides and amorphous high-valance NiFe hydroxide nanosheets enhancing oxygen evolution reaction. *Chem Eng J*. 2022;430:133047.

126. Zhao J, Wang J, Chen Z, Ju J, Han X, Deng Y. Metal chalcogenides: an emerging material for electrocatalysis. *APL Mater*. 2021;9(5):050902.
127. Yin J, Jin J, Lin H, et al. Optimized metal chalcogenides for boosting water splitting. *Adv Sci*. 2020;7(10):1903070.
128. Chen Z, Wei W, Ni B-J. Cost-effective catalysts for renewable hydrogen production via electrochemical water splitting: recent advances. *Curr Opin Green Sustainable Chem*. 2021;27:100398.
129. Zheng R, Li J, Zhu R, et al. Enhanced Cr(VI) reduction on natural chalcopyrite mineral modulated by degradation intermediates of RhB. *J Hazard Mater*. 2021;423:127206.
130. Kale SB, Bhardwaj A, Lokhande VC, et al. Amorphous cobalt-manganese sulfide electrode for efficient water oxidation: meeting the fundamental requirements of an electrocatalyst. *Chem Eng J*. 2021;405:126993.
131. Jia X, Kang H, Yang X, et al. Amorphous Ni(III)-based sulfides as bifunctional water and urea oxidation anode electrocatalysts for hydrogen generation from urea-containing water. *Appl Catal B: Environ*. 2022;312:121389.
132. Qin C, Fan A, Ren D, et al. Amorphous NiMS (M: Co, Fe or Mn) holey nanosheets derived from crystal phase transition for enhanced oxygen evolution in water splitting. *Electrochim Acta*. 2019;323:134756.
133. Dong Y, Fang Z, Yang W, Tang B, Liu Q. Integrated bifunctional electrodes based on amorphous Co–Ni–S nanoflake arrays with atomic dispersity of active sites for overall water splitting. *ACS Appl Mater Interfaces*. 2022;14(8):10277-10287.
134. Chen Z, Ibrahim I, Hao D, et al. Controllable design of nanoworm-like nickel sulfides for efficient electrochemical water splitting in alkaline media. *Mater Today Energy*. 2020;18:100573.
135. Wang F, Zhang K, Zha Q, Ni Y. Honeycomb-like Ni-Mo-S on Ni foam as superior bifunctional electrocatalyst for hydrogen evolution and urea oxidation. *J Alloys Compd*. 2022;899:163346.
136. Cai P, Huang J, Chen J, Wen Z. Oxygen-containing amorphous cobalt sulfide porous nanocubes as high-activity electrocatalysts for the oxygen evolution reaction in an alkaline/neutral medium. *Angew Chem Int Ed*. 2017;56(17):4858-4861.
137. Shao Z, Meng H, Sun J, et al. Engineering of amorphous structures and sulfur defects into ultrathin FeS nanosheets to achieve superior electrocatalytic alkaline oxygen evolution. *ACS Appl Mater Interfaces*. 2020;12(46):51846-51853.
138. Deng X, Li H, Huang J, Li Y. Controllable in situ growth of amorphous MoS_x nanosheets on CoAl layered double hydroxides for efficient oxygen evolution reaction. *Electrochem Commun*. 2020;110:106634.
139. Feng X, Jiao Q, Zhang J, et al. Integrating amorphous molybdenum sulfide nanosheets with a Co_9S_8@Ni_3S_2 array as an efficient electrocatalyst for overall water splitting. *Langmuir*. 2022;38(11):3469-3479.
140. Yan Y, Ge X, Liu Z, Wang J-Y, Lee J-M, Wang X. Facile synthesis of low crystalline MoS_2 nanosheet-coated CNTs for enhanced hydrogen evolution reaction. *Nanoscale*. 2013;5(17):7768-7771.
141. Liu Y, Li Q, Si R, et al. Coupling sub-nanometric copper clusters with quasi-amorphous cobalt sulfide yields efficient and robust electrocatalysts for water splitting reaction. *Adv Mater*. 2017;29(13):1606200.
142. Niu Y, Li W, Wu X, et al. Amorphous nickel sulfide nanosheets with embedded vanadium oxide nanocrystals on nickel foam for efficient electrochemical water oxidation. *J Mater Chem A*. 2019;7(17):10534-10542.
143. Xu Y-Z, Yuan C-Z, Chen X-P. One-pot synthesis nickel sulfide/amorphous molybdenum sulfide nanosheets array on nickel foam as a robust oxygen evolution reaction electrocatalyst. *J Solid State Chem*. 2017;256:124-129.
144. Li Z, Wang X, Wang X, et al. Mn-Cd-S@amorphous-Ni_3S_2 hybrid catalyst with enhanced photocatalytic property for hydrogen production and electrocatalytic OER. *Appl Surf Sci*. 2019;491:799-806.
145. Song S, Wang Y, Li W, et al. Amorphous MoS_2 coated Ni_3S_2 nanosheets as bifunctional electrocatalysts for high-efficiency overall water splitting. *Electrochim Acta*. 2020;332:135454.
146. Chen N, Du Y-X, Zhang G, Lu W-T, Cao F-F. Amorphous nickel sulfoselenide for efficient electrochemical urea-assisted hydrogen production in alkaline media. *Nano Energy*. 2021;81:105605.
147. Chen Z, Wei W, Ni B-J. Transition metal chalcogenides as emerging electrocatalysts for urea electrolysis. *Curr Opin Electrochem*. 2022;31:100888.
148. Xu X, Du P, Chen Z, Huang M. An electrodeposited cobalt–selenide-based film as an efficient bifunctional electrocatalyst for full water splitting. *J Mater Chem A*. 2016;4(28):10933-10939.
149. Yang W, Hua Y, Zhang Q, Lei H, Xu C. Electrochemical fabrication of 3D quasi-amorphous pompon-like Co-O and Co-Se hybrid films from choline chloride/urea deep eutectic solvent for efficient overall water splitting. *Electrochim Acta*. 2018;273:71-79.
150. Pang Y, Xu W, Zhu S, et al. Self-supporting amorphous nanoporous NiFeCoP electrocatalyst for efficient overall water splitting. *J Mater Sci Technol*. 2021;82:96-104.
151. Zhao S, Zhao Y, Chen J, et al. Crystalline and amorphous phases: niFeCo tri-metal phosphide as an efficient electrocatalyst to accelerate oxygen evolution reaction kinetics. *Electrochim Acta*. 2022;426:140788.
152. Li L, Huang W, Lei J, Shang B, Li N, Pan F. Holey nanospheres of amorphous bimetallic phosphide electrodeposited on 3D porous Ni foam for efficient oxygen evolution. *Appl Surf Sci*. 2019;479:540-547.
153. Yu X, He X, Li R, Gou X. One-step synthesis of amorphous nickel iron phosphide hierarchical nanostructures for water electrolysis with superb stability at high current density. *Dalton Trans*. 2021;50(23):8102-8110.
154. Barati Darband G, Maleki M, Toghraei A, Shanmugam S. Electrodeposition of self-supported transition metal phosphides nanosheets as efficient hydrazine-assisted electrolytic hydrogen production catalyst. *Int J Hydrogen Energy*. 2023;48(11):4253-4263.
155. Jiang S, Zhu L, Yang Z, Wang Y. Enhanced electrocatalytic performance of FeNiCoP amorphous alloys as oxygen-evolving catalysts for electrolytic water splitting application. *Electrochim Acta*. 2021;368:137618.
156. Chunduri A, Gupta S, Bapat O, et al. A unique amorphous cobalt-phosphide-boride bifunctional electrocatalyst for enhanced alkaline water-splitting. *Appl Catal B: Environ*. 2019;259:118051.
157. Wang T, Wang C, Jin Y, et al. Amorphous Co–Fe–P nanospheres for efficient water oxidation. *J Mater Chem A*. 2017;5(48):25378-25384.

158. Huang H, Cho A, Kim S, et al. Structural design of amorphous $CoMoP_x$ with abundant active sites and synergistic catalysis effect for effective water splitting. *Adv Funct Mater*. 2020;30(43):2003889.
159. Pawar SM, Pawar BS, Babar PT, et al. Electrosynthesis of copper phosphide thin films for efficient water oxidation. *Mater Lett*. 2019;241:243-247.
160. Zhang W, Li Y, Zhou L, et al. Ultrathin amorphous CoFeP nanosheets derived from CoFe LDHs by partial phosphating as excellent bifunctional catalysts for overall water splitting. *Electrochim Acta*. 2019;323:134595.
161. Xu Y, Cheng Z, Jiang J, Du J, Xu Q. 2D amorphous bi-metallic NiFe nitrides for a high-efficiency oxygen evolution reaction. *Chemical Commun*. 2021;57(97):13170-13173.
162. Liu G, Wu Y, Yao R, Zhao F, Zhao Q, Li J. Amorphous iron-nickel phosphide nanocone arrays as efficient bifunctional electrodes for overall water splitting. *Green Energy Environ*. 2021;6(4):496-505.
163. Jiang H, Sun M, Wu S, Huang B, Lee CS, Zhang W. Oxygen-incorporated NiMoP nanotube arrays as efficient bifunctional electrocatalysts for urea-assisted energy-saving hydrogen production in alkaline electrolyte. *Adv Funct Mater*. 2021;31(43):2104951.
164. Zou H, Li G, Duan L, Kou Z, Wang J. In situ coupled amorphous cobalt nitride with nitrogen-doped graphene aerogel as a trifunctional electrocatalyst towards Zn-air battery deriven full water splitting. *Appl Catal B: Environ*. 2019;259:118100.
165. Li R, Xu J, Lu C, et al. Amorphous NiFe phosphides supported on nanoarray-structured nitrogen-doped carbon paper for high-performance overall water splitting. *Electrochim Acta*. 2020;357:136873.
166. Song H, Yu J, Tang Z, Yang B, Lu S. Halogen-doped carbon dots on amorphous cobalt phosphide as robust electrocatalysts for overall water splitting. *Adv Energy Mater*. 2022;12(14):2102573.
167. Zhou H, Zheng M, Pang H. Synthesis of hollow amorphous cobalt phosphide-cobalt oxide composite with interconnected pores for oxygen evolution reaction. *Chem Eng J*. 2021;416:127884.
168. Xu X, Li C, Lim JG, et al. Hierarchical design of NiOOH@amorphous Ni–P bilayer on a 3D mesh substrate for high-efficiency oxygen evolution reaction. *ACS Appl Mater Interfaces*. 2018;10(36):30273-30282.
169. Meena A, Thangavel P, Jeong DS, et al. Crystalline-amorphous interface of mesoporous Ni_2P@ $FePO_xH_y$ for oxygen evolution at high current density in alkaline-anion-exchange-membrane water-electrolyzer. *Appl Catal B: Environ*. 2022;306:121127.
170. Zhang L, Ding X, Cong M, Wang Y, Zhang X. Self-adaptive amorphous Co_2P@Co_2P/Co-polyoxometalate/nickel foam as an effective electrode for electrocatalytic water splitting in alkaline electrolyte. *Int J Hydrogen Energy*. 2019;44(18):9203-9209.
171. Liu G, He D, Yao R, Zhao Y, Li J. Amorphous NiFeB nanoparticles realizing highly active and stable oxygen evolving reaction for water splitting. *Nano Res*. 2018;11(3):1664-1675.
172. Li Y, Huang B, Sun Y, et al. Multimetal borides nanochains as efficient electrocatalysts for overall water splitting. *Small*. 2019;15(1):1804212.
173. Nsanzimana JMV, Gong L, Dangol R, et al. Tailoring of metal boride morphology via anion for efficient water oxidation. *Adv Energy Mater*. 2019;9(28):1901503.
174. Nsanzimana JMV, Reddu V, Peng Y, Huang Z, Wang C, Wang X. Ultrathin amorphous iron–nickel boride nanosheets for highly efficient electrocatalytic oxygen production. *Chem Eur J*. 2018;24(69):18502-18511.
175. Chen Z, Zheng R, Zou W, et al. Integrating high-efficiency oxygen evolution catalysts featuring accelerated surface reconstruction from waste printed circuit boards via a boriding recycling strategy. *Appl Catal B: Environ*. 2021;298:120583.
176. Tripathy RK, Samantara AK, Behera JN. Electrochemically activated Co-Prussian blue analogue derived amorphous CoB nanostructures: an efficient electrocatalyst for the oxygen evolution reaction. *Dalton Trans*. 2022;51(7):2782-2788.
177. He T, Nsanzimana JMV, Qi R, et al. Synthesis of amorphous boride nanosheets by the chemical reduction of Prussian blue analogs for efficient water electrolysis. *J Mater Chem A*. 2018;6(46):23289-23294.
178. Wang S, Zhao R, Zheng T, Fang Y, Wang W, Xue W. Metal-organic framework-derived self-supporting metal boride for efficient electrocatalytic oxygen evolution reaction. *J Colloid Interface Sci*. 2022;618:34-43.
179. Li Y, Jiang X, Tang M, et al. A high-performance oxygen evolution electrocatalyst based on partially amorphous bimetallic cobalt iron boride nanosheet. *Int J Hydrogen Energy*. 2020;45(53):28586-28597.
180. Nsanzimana JMV, Peng Y, Xu YY, et al. An efficient and earth-abundant oxygen-evolving electrocatalyst based on amorphous metal borides. *Adv Energy Mater*. 2018;8:1701475.
181. Sun Y, Zhao Y, Deng X, Dai D, Gao H. An efficient amorphous ternary transition metal boride (WFeNiB) electrocatalyst for oxygen evolution from water. *Sustainable Energy Fuels*. 2022;6(5):1345-1352.
182. Chen H, Ouyang S, Zhao M, Li Y, Ye J. Synergistic activity of Co and Fe in amorphous Co_x–Fe–B catalyst for efficient oxygen evolution reaction. *ACS Appl Mater Interfaces*. 2017;9(46):40333-40343.
183. Cai W, Yang H, Zhang J, et al. Amorphous multimetal alloy oxygen evolving catalysts. *ACS Mater Lett*. 2020;2(6):624-632.
184. Tang W, Liu X, Li Y, et al. Boosting electrocatalytic water splitting via metal-metalloid combined modulation in quaternary Ni-Fe-PB amorphous compound. *Nano Res*. 2020;13(2):447-454.
185. Ren H, Sun X, Du C, et al. Amorphous Fe–Ni–P–B–O nanocages as efficient electrocatalysts for oxygen evolution reaction. *ACS Nano*. 2019;13(11):12969-12979.
186. ul Haq T, Mansour SA, Munir A, Haik Y. Gold-supported gadolinium doped CoB amorphous sheet: a new benchmark electrocatalyst for water oxidation with high turnover frequency. *Adv Funct Mater*. 2020;30(16):1910309.
187. Wang S, Zhao R, Zheng T, et al. Cerium decorated amorphous ternary Ni-Ce-B catalyst for enhanced electrocatalytic water oxidation. *Surf Interfaces*. 2021;26:101447.
188. Lu Y, Wang J, Peng Y, Fisher A, Wang X. Highly efficient and durable Pd hydride nanocubes embedded in 2D amorphous NiB nanosheets for oxygen reduction reaction. *Adv Energy Mater*. 2017;7(21):1700919.
189. Nsanzimana JMV, Dangol R, Reddu V, et al. Facile synthesis of amorphous ternary metal borides-reduced graphene oxide hybrid with superior oxygen evolution activity. *ACS Appl Mater Interfaces*. 2019;11(1):846-855.

190. Suliman M, Suliman M, Adam A, Basheer C, Yamani Z, Qamar M. Interfacial coupling of amorphous cobalt boride with g-C_3N_4 nanosheets for superior oxygen evolution reaction. *Mater Lett*. 2020;268:127593.
191. Suliman MA, Basheer C, Farooq W. Cobalt boride/g-C_3N_4 nanosheets-assisted electrocatalytic oxidation of 5-hydroxymethylfurfural into 2, 5-furandicarboxylic acid. *Catalysts*. 2021;11(10):1241.
192. Xie T, Song G, Wang G, et al. Amorphous iron boride in situ grown on black phosphorus sheets: a promising electrocatalyst for OER. *J Electron Mater*. 2022;51(7):3705-3713.
193. Sukanya R, Chen S-M. Amorphous cobalt boride nanosheets anchored surface-functionalized carbon nanofiber: an bifunctional and efficient catalyst for electrochemical sensing and oxygen evolution reaction. *J Colloid Interface Sci*. 2020;580:318-331.
194. Chen Z, Zheng R, Wei W, et al. Recycling spent water treatment adsorbents for efficient electrocatalytic water oxidation reaction. *Resour Conserv Recycl*. 2022;178:106037.
195. Graś M, Kolanowski Ł, Chen Z, et al. Partial inhibition of borohydride hydrolysis using porous activated carbon as an effective method to improve the electrocatalytic activity of the DBFC anode. *Sustainable Energy Fuels*. 2021;5(17):4401-4413.
196. Hong Y-R, Kim KM, Ryu JH, et al. Dual-phase engineering of nickel boride-hydroxide nanoparticles toward high-performance water oxidation electrocatalysts. *Adv Funct Mater*. 2020;30(38):2004330.
197. Li T, Jing T, Rao D, et al. In situ coating amorphous boride on ternary pyrite-type boron sulfide for highly efficient oxygen evolution. *J Mater Chem A*. 2021;9(20):12283-12290.
198. Sun Z, Wang X, Yuan M, et al. "Lewis base-hungry" amorphous–crystalline nickel borate–nickel sulfide heterostructures by in situ structural engineering as effective bifunctional electrocatalysts toward overall water splitting. *ACS Appl Mater Interfaces*. 2020;12(21):23896-23903.
199. Zhang L, Lu C, Ye F, et al. Vacancies boosting strategy enabling enhanced oxygen evolution activity in a library of novel amorphous selenite electrocatalysts. *Appl Catal B: Environ*. 2021;284:119758.
200. Meng Y, Ni G, Jin X, Peng J, Yan Q. Recent advances in the application of phosphates and borates as electrocatalysts for water oxidation. *Mater Today Nano*. 2020;12:100095.
201. Zhao W, Xu T, Li T, et al. Amorphous iron(III)-borate nanolattices as multifunctional electrodes for self-driven overall water splitting and rechargeable zinc–air battery. *Small*. 2018;14(48):1802829.
202. Amer MS, Arunachalam P, Alsalman AM, et al. Facile synthesis of amorphous nickel iron borate grown on carbon paper as stable electrode materials for promoted electrocatalytic urea oxidation. *Catal Today*. 2022;397-399:197-205.
203. Dong Y, Zhao T, Zhong D, et al. Amorphous CoV phosphate nanosheets as efficient oxygen evolution electrocatalyst. *Chem Asian J*. 2022;17(10):e202200126.
204. Zhou Y, Zeng HC. 3D networks of CoFePi with hierarchical porosity for effective OER electrocatalysis. *Small*. 2018;14(21):1704403.
205. Guo X, Xu Y, Cheng Y, Zhang Y, Pang H. Amorphous cobalt phosphate porous nanosheets derived from two-dimensional cobalt phosphonate organic frameworks for high performance of oxygen evolution reaction. *Appl Mater Today*. 2020;18:100517.
206. Sial MAZG, Lin H, Wang X. Microporous 2D NiCoFe phosphate nanosheets supported on Ni foam for efficient overall water splitting in alkaline media. *Nanoscale*. 2018;10(27):12975-12980.
207. Dastafkan K, Li Y, Zeng Y, Han L, Zhao C. Enhanced surface wettability and innate activity of an iron borate catalyst for efficient oxygen evolution and gas bubble detachment. *J Mater Chem A*. 2019;7(25):15252-15261.
208. Ge J, Lai Y, Guan M, Xiao Y, Kuang J, Yang C. Nickel borate with a 3D hierarchical structure as a robust and efficient electrocatalyst for urea oxidation. *Environ Sci: Nano*. 2021;8(5):1326-1335.
209. Zhang J, Tan X, Wang W, Cao L, Dong B. Iron-doped cobalt phosphate 1D amorphous ultrathin nanowires as a highly efficient electrocatalyst for water oxidation. *Sustainable Energy Fuels*. 2020;4(9):4704-4712.
210. Wang R, Li Y, Tan X, et al. Amorphous doping promotes utilization of Fe-doped amorphous $Zr(HPO_4)_2$ for superb water oxidation electrocatalysis. *Adv Mater Interfaces*. 2022;9(15):2200387.
211. Ji X, Ren X, Hao S, et al. Remarkable enhancement of the alkaline oxygen evolution reaction activity of $NiCo_2O_4$ by an amorphous borate shell. *Inorg Chem Front*. 2017;4(9):1546-1550.
212. Tan T, Han P, Cong H, Cheng G, Luo W. An amorphous cobalt borate nanosheet-coated cobalt boride hybrid for highly efficient alkaline water oxidation reaction. *ACS Sustainable Chem Eng*. 2019;7(6):5620-5625.
213. Zhang L, Zhang R, Ge R, et al. Facilitating active species generation by amorphous NiFe-Bi layer formation on NiFe-LDH nanoarray for efficient electrocatalytic oxygen evolution at alkaline pH. *Chem Eur J*. 2017;23(48):11499-11503.
214. Chen P, Xu K, Zhou T, et al. Strong-coupled cobalt borate nanosheets/graphene hybrid as electrocatalyst for water oxidation under both alkaline and neutral conditions. *Angew Chem Int Ed*. 2016;55(7):2488-2492.
215. Liu X, Yin Q, Dai C, et al. Amorphous bimetallic phosphate–carbon precatalyst with deep self-reconstruction toward efficient oxygen evolution reaction and Zn–air batteries. *ACS Sustainable Chem Eng*. 2021;9(15):5345-5355.

How to cite this article: Chen Z, Han N, Zheng R, Ren Z, Wei W, Ni B-J. Design of earth-abundant amorphous transition metal-based catalysts for electrooxidation of small molecules: Advances and perspectives. *SusMat*. 2023;3:290–319. https://doi.org/10.1002/sus2.131

AUTHOR BIOGRAPHIES

Zhijie Chen received his Ph.D. degree in Environmental Engineering from the University of Technology Sydney (UTS), Australia in 2022. He now works as a Postdoc researcher at the Centre for Technology in Water and Wastewater (CTWW), School of Civil and Environmental Engineering, UTS. His research work mainly focuses on waste valorization and eco-design of cost-effective materials for advanced energy and environmental applications (e.g., water electrolysis and wastewater purification/reutilization).

Bing-Jie Ni received his Ph.D. degree in environmental engineering in June 2009. He currently is a full professor in environmental engineering. He has been working in the field of renewable energy production, particularly the interface between chemical engineering and environmental technology. His work focuses on the integration of these disciplines to develop innovative and sustainable technological solutions to achieve efficient energy generation from renewable resources.